Evapotranspiration over agroforestry sites in Germany

Christian Markwitz[1], Alexander Knohl[1,2], and Lukas Siebicke[1]

[1]University of Goettingen, Bioclimatology, Faculty of Forest Sciences and Forest Ecology, Germany
[2]University of Goettingen, Centre of Biodiversity and Sustainable Land Use (CBL), Germany

Correspondence: Christian Markwitz (christian.markwitz@forst.uni-goettingen.de)

Abstract. In past years the interest in growing crops and trees for bioenergy production increased. One agricultural practice is the mixed cultivation of fast growing trees and annual crops or perennial grass-lands on the same piece of land, referred to as one type of agroforestry (AF). The inclusion of tree strips into the agricultural landscape has been shown - on the one hand - to lead to reduced wind speeds and higher carbon sequestration above-ground and in the soil. On the other hand, concerns have been risen about increased water losses to the atmosphere via evapotranspiration (ET). Therefore we hypothesize that short rotation coppice agroforestry systems have higher water losses to the atmosphere via ET, compared to monoculture agriculture without trees (MC). In order to test the hypothesis the main objective was to measure actual evapotranspiration of five AF systems in Germany and compare those to five monoculture systems in close vicinity to the AF systems.

We measured actual ET at five AF sites in direct comparison to five monoculture (MC) sites in Northern Germany in 2016 and 2017. We used an eddy covariance energy balance set-up (ECEB) and a low-cost eddy covariance set-up (EC-LC) to measure actual ET over each AF and each MC system. We conducted direct eddy covariance (EC) measurement campaigns of approximately four weeks duration for method validation.

Results from the short-term measurement campaigns showed a high agreement between $\mathrm{ET_{EC-LC}}$ and $\mathrm{ET_{EC}}$, indicated by slopes of a linear regression analysis between 0.86 and 1.3 (R^2 between 0.7 and 0.94) across sites. Root mean square errors of $\mathrm{LE_{EC-LC}}$ vs. $\mathrm{LE_{EC}}$ were half as small as $\mathrm{LE_{ECEB}}$ vs. $\mathrm{LE_{EC}}$, indicating a superior agreement of the EC-LC set-up with the EC set-up compared to the ECEB set-up.

With respect to the annual sums of ET over AF and MC, we observed small differences between the two land-uses. We interpret this as an effect of compensating small-scale differences in ET next to and in between the tree strips for ET measurements on system-scale. Most likely, differences in ET rates next to and in between the tree strips are of the same order of magnitude but of opposite sign and compensate each other throughout the year. Differences between annual sums of ET from the two methods were of the same order of magnitude as differences between the two land-uses. Compared to the effect of land-use and different methods on ET, we found larger mean evapotranspiration indices ($\sum$ET/$\sum$P) across sites for a drier than normal year (2016) compared to a wet year (2017). This indicates that we were able to detect differences in ET due to different ambient conditions with the applied methods, rather than the potentially small effect of AF on ET.

We conclude that agroforestry has not resulted in an increased water loss to the atmosphere indicating that agroforestry in Germany can be a land-use alternative to monoculture agriculture without trees.

Copyright statement. TEXT

1 Introduction

In past years the interest in growing crops and trees for the production of bioenergy has increased, especially in the scope of climate change mitigation and carbon sequestration (Fischer et al., 2013; Zenone et al., 2015). One method of efficient biomass production is the cultivation of short rotation coppice (SRC), referred to as ”any high-yielding woody species managed in a coppice system“ (Aylott et al., 2008). Typically, fast growing tree species, such as poplar or willow are used for SRC plantations. The trees are commonly harvested after a three to five year rotation period and used for energy and heat production (Aylott et al., 2008). SRC plantations are monoculture systems with a single tree species grown.

The cultivation of fast growing trees with annual crops or perennial grass-lands on the same piece of land is an example of agroforestry (AF) (Morhart et al., 2014; Smith et al., 2013) and has numerous environmental benefits relative to monoculture (MC) systems consisting only of crops or grasses without trees (Quinkenstein et al., 2009). De Stefano and Jacobson (2018) found that the inclusion of fast growing trees arranged into tree strips (short rotation alley cropping agroforestry) leads to a higher carbon sequestration above-ground and in the soil relative to monoculture systems. The additional biomass input from litter, dead wood and roots led to increased soil fertility (e.g. Beuschel et al. (2018); Quinkenstein et al. (2009); Tsonkova et al. (2012)). Böhm et al. (2014) and Kanzler et al. (2018) reported reduced wind velocity leewards of the tree strips when oriented perpendicular to the prevailing wind direction. In addition, Cleugh (1998) and Quinkenstein et al. (2009) found that tree strips reduce incident solar radiation, leading to reduced air temperature (McNaughton, 1988). Effects of tree strips on microclimate are mostly attributed to a region next to the tree strips with the extent depending on tree strip properties, such as the space between the tree strips, their orientation relative to the prevailing wind direction, their density, height and width (Quinkenstein et al., 2009).

Evapotranspiration (ET) in AF is strongly affected by the tree strip properties and is the combined process of 1) evaporation from the soil and open water from leaf surfaces and 2) leaf transpiration (Katul et al., 2012). ET within AF is reduced on the downwind side of the tree strips caused by a wind velocity reduction (Cleugh, 1998; Davis and Norman, 1988; Kanzler et al., 2018; Quinkenstein et al., 2009; Tsonkova et al., 2012). Davis and Norman (1988) explained the reduction in ET by the protection of adjacent crops from dry air advection. The reduced dry air advection leads to a decreased vapour pressure deficit (D), lowering ET (Kanzler et al., 2018). The potential reduction in ET in the vicinity of the tree strips leads to an increased soil water content downwind, with the potential for enhancing yield production (Kanzler et al., 2018; Swieter et al., 2019).

Currently, little is known about system-scale water use of heterogeneously shaped short rotation alley cropping agroforestry systems in Germany. The majority of previous studies focused on the water use of short rotation coppices, but not AF systems (Bloemen et al., 2016; Fischer et al., 2013; Schmidt-Walter et al., 2014; Fischer et al., 2018). Fischer et al. (2013) and Zenone et al. (2015) observed a lower annual sum of evapotranspiration over a poplar SRC in the Czech Republic and in Belgium compared to the annual sum of evapotranspiration over a reference grassland. This is contradictory to the assumption that SRC plantations are strong water consumers. For AF systems we formulated the same hypothesis, i.e. system-scale evapotranspiration over AF systems is higher compared to monoculture agriculture without trees.

However, the effect of AF on system-scale evapotranspiration is site specific and depends on the local climate, the soil type, the water availability and the AF design. Therefore, repeated measurements at different sites are essential for studies on the effects of AF on evapotranspiration. Nevertheless, this requires methods of low maintenance with low power consumption, and moderate cost.

The most common approach for evapotranspiration measurements at ecosystem scale is the eddy covariance (EC) method (Baldocchi, 2003, 2014). EC provides a tool for real time flux measurements on a time scale of 30 minutes. The complexity and cost of traditional EC systems, however, usually limits the required replication of measurement units (Hill et al., 2017). An alternative method with lower costs is the eddy covariance energy balance method (ECEB) (Amiro, 2009). The latent heat flux (LE) is calculated as the residual of the energy balance components, i.e., the net radiation, the ground heat flux, the sensible heat flux and various storage terms. The ECEB method is limited by the accuracy of the energy balance components, typically leading to an overestimation of latent heat fluxes. Therefore, we need to assess to what extent the energy balance is closed at the given sites. Another alternative method for measurements of evapotranspiration is the use of slower but cheaper humidity sensors resulting in a low-cost eddy covariance set-up (EC-LC) (Markwitz and Siebicke, 2019). The measurement principle follows the concept of the eddy covariance method, however, the fast response gas analyser is replaced by a slow response thermohygrometer. The slow response time of the humidity sensor limits the sampling of turbulent eddies across the whole energy spectrum, which we address by appropriate high-frequency corrections during preprocessing. For latent heat fluxes obtained by EC-LC the non-closure of the energy balance causes a flux underestimation as observed for traditional EC set-ups. Any potential non-closure we then address by direct measurements of the latent heat flux to estimate the energy balance non-closure and partition the residual energy to the sensible and latent heat flux.

The main hypothesis of the current work was that short rotation alley cropping AF systems have higher water losses to the atmosphere via ET, compared to monoculture agriculture without trees. In order to test the hypothesis the main objectives of the study are (1) to evaluate the eddy covariance energy balance (ECEB) and low-cost eddy covariance (EC-LC) method against direct eddy covariance (EC) measurements, and (2) to measure actual evapotranspiration of five AF systems in Germany and compare those to five monoculture systems in close vicinity to the AF systems using the two different approaches.

2 Materials and methods

2.1 Site description

This study was carried out as part of the project ‘Sustainable Intensification of Agriculture through Agroforestry’ (SIGNAL, http://signal.uni-goettingen.de/, last access: 19 January 2020), investigating the sustainability of AF systems in Germany. We performed measurements at five sites across Northern Germany (Fig. 1 left). Each site consisted of one AF system and one monoculture (MC) system (Fig. 1 for an aerial photograph of the Dornburg, Forst, Mariensee, Reiffenhausen and Wendhausen site with AF and MC selected). The AF systems are of a short rotation alley cropping type, with fast growing trees interleaved by either crops (Fig. 1 for images of the cropland AF systems in Dornburg, Forst and Wendhausen) or perennial grasslands (Fig. 1 for images of the grassland AF systems in Mariensee and Reiffenhausen). The crops and grasses at the monoculture systems undergo the same tillage and fertilization as the crops and grasses cultivated between the tree strips. The MC system serves as a reference to the AF system. Table 1 specifies the site locations and the AF geometry.

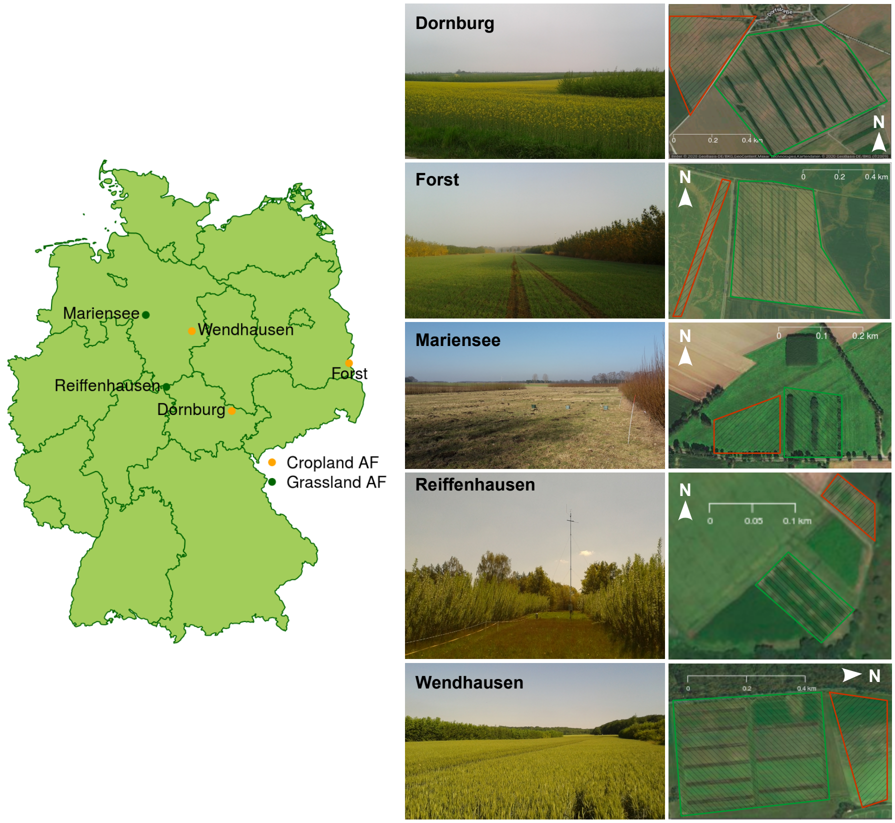

Figure 1. Left: map of SIGNAL sites, with the respective AF type of either cropland or grassland AF; **Right:** image and aerial photograph of the AF systems. Green hatched areas in the aerial photograph correspond to the area of the AF system and red hatched areas correspond to the area of the MC system. Site images are own photographs and aerial photographs originate from Google maps/ Google earth ©Google 2020.

2.2 Measurements

Measurements of meteorological and micrometeorological variables were performed since March 2016. At each AF system we installed an eddy covariance mast with a height of 10 m and at each MC system an eddy covariance mast with a height of 3.5 m. Each mast was equipped with the same meteorological and micrometeorological instrumentation. The standard set-up consisted of instruments measuring wind speed, wind direction, sensible heat flux, net radiation, global radiation, air temperature, relative

Table 1. Site locations and AF geometry.

Site	Coordinates	No. of tree strips	Distance between tree strips (m)	Orientation of tree strips	Tree height (m)	Agroforestry type	Agroforestry system size (ha)	Relative tree cover (%)
Reiffenhausen	51°24'N 9°59'E	3	9	NW-SE	4.73±0.32 (n=69) Malec (2017)	Willow-grassland	1.9	72
Mariensee	52°34'N 9°28'E	3	48	N-S	4.01±0.33 (n=96) Swieter and Langhof (2017)	Willow-grassland	7	6
Wendhausen	52°20'N 10°38'E	6	24, 48, 96	N-S	6.21±0.4 (n=114) Swieter and Langhof (2017)	Poplar-cropland	18	11.52
Forst	51°47'N 14°38'E	7	24, 48, 96	N-S	6.5±1.8 (n=161) Seserman (2017)	Poplar-cropland	39.1	12
Dornburg	51°00'N 11°38'E	7	48, 96, 125	NW-SE	6.4±0.64 (n=160) Rudolf (2017)	Poplar-cropland	51	8

humidity, precipitation and ground heat flux. An overview of the installed instruments and the respective variables used for the presented set-ups is given in Table 2.

Gaps in precipitation measurements at all sites were filled by precipitation data collected at nearby weather stations operated by the German weather service (DWD). We used the R-package rdwd (Boessenkool, 2019) for data download from the ftp server maintained by the DWD. We replaced gaps in precipitation measurements with DWD data if more than 25 % of precipitation data per day were missing. We used precipitation data from the weather stations Erfurt-Weimar airport, Cottbus, Hannover-Herrenhausen and Braunschweig to fill data gaps in precipitation at Dornburg, Forst, Mariensee and Wendhausen, respectively. In Reiffenhausen we used the precipitation records of a station placed at the same site and operated by the soil hydrology group at the University of Göttingen. As the precipitation transmitter was placed inside or next to the tree strips at the majority of the AF systems, the measurements were affected by interception and were lower than at the MC system. Therefore, we used the precipitation measurements from the MC system to compute ratios of annually summed actual ET and net radiation to precipitation at both AF and MC systems. We assume that the annual sum of precipitation at the AF and the MC systems do not differ, due to the relatively small size of the AF systems and no expected local effects of the AF systems on the precipitation formation.

In the following sections we briefly describe the concepts of the used set-ups, eddy covariance (EC), eddy covariance energy-balance (ECEB) and low-cost eddy covariance (EC-LC). Throughout the paper we use the respective abbreviations.

2.2.1 Eddy Covariance (EC)

Sensible heat and momentum fluxes have been measured continuously with ultrasonic anemometers since 2016. The water vapour and CO_2 mole fraction were measured during field campaigns during the vegetation periods of 2016 and 2017 (Table A1). During the field campaigns the standard set-up was extended by an enclosed-path infrared gas analyser (LI-7200 , LI-COR Inc., Lincoln, Nebraska, USA). In 2016, the campaigns were conducted separately at the AF and MC systems with

Table 2. Instrumentation for flux and meteorological measurements used at all five AF and MC systems. Set-up corresponds to eddy covariance, EC, low-cost eddy covariance, EC-LC, and eddy covariance energy balance, ECEB.

Variable	Height (m)	Instrument	Company	Set-up
3D wind components, u, v, w ($\mathrm{m\,s^{-1}}$) ultrasonic temperature, T_s (°C), wind speed ($\mathrm{m\,s^{-1}}$), -direction (°)	3.5,10	uSONIC-3 Omni	METEK GmbH Elmshorn, Germany	EC, ECEB, EC-LC
Net radiation, R_N ($\mathrm{W\,m^{-2}}$)	3, 9.5	NR-Lite2 Net Radiometer	Kipp&Zonen Delft, The Netherlands	ECEB
Global radiation, R_G ($\mathrm{W\,m^{-2}}$)	3, 9.5	CMP3 Pyranometer	Kipp&Zonen Delft, The Netherlands	
Relative humidity, RH (%), air temperature, T (°C)	2	Hygro-Thermo Transmitter-compact (Model 1.1005.54.160)	Thies Clima Göttingen, Germany	EC, ECEB
RH, T, Atmospheric pressure, P_A (Pa)	0.5, 3/9.5	BME280	BOSCH, Germany	EC-LC
Precipitation, P (mm)	1	Precipitation Transmitter (Model 5.4032.35.007)	Thies Clima Göttingen, Germany	
P_A	0.5, 1.5	Baro Transmitter (Model 3.1157.10.000)	Thies Clima Göttingen, Germany	EC, ECEB, EC-LC
Ground heat flux, G ($\mathrm{W\,m^{-2}}$)	-0.05	Hukseflux HFP01	Hukseflux Delft, The Netherlands	ECEB
Soil temperature, T_{Soil} (°C)	-0.02, -0.05, -0.10, -0.25, -0.5	DS18B20		ECEB, EC-LC
Water vapour mole fraction, $C_{H_2O_v}$ ($\mathrm{mmol\,mol^{-1}}$)	3.5, 10	LI-7200	LI-COR Inc. Lincoln, Nebraska (USA)	EC
Carbon dioxide mole fraction, C_{CO_2} ($\mathrm{\mu mol\,mol^{-1}}$)	3.5, 10	LI-7200	LI-COR Inc. Lincoln, Nebraska (USA)	EC

one available gas analyser, whilst in 2017 both systems were sampled simultaneously with two available gas analyser. Data processing and the analysis procedure is described in more detail in Markwitz and Siebicke (2019).

2.2.2 Eddy Covariance Energy-Balance (ECEB)

The energy balance at the surface is

$$R_N - G = H + LE + S \tag{1}$$

with net radiation, R_N ($\mathrm{W\,m^{-2}}$), ground heat flux, G ($\mathrm{W\,m^{-2}}$), sensible heat flux, H ($\mathrm{W\,m^{-2}}$), latent heat flux, LE ($\mathrm{W\,m^{-2}}$), and soil storage flux, S ($\mathrm{W\,m^{-2}}$). By convention a turbulent flux towards the atmosphere is defined as positive and a turbulent flux towards the surface is defined as negative. A positive net radiation corresponds to a surplus of radiative energy at the surface and a positive ground heat flux describes a heat transport into the soil. LE from ECEB (LE_{ECEB}) was calculated as the residual of the net radiation, the ground- and sensible heat flux, and the soil storage flux according to Eq. (1)

$$LE_{ECEB} = R_N - G - H - S \tag{2}$$

assuming a fully closed surface energy balance. The conversion of LE into ET and the derivation of the soil storage flux are given in Section A1.

The energy balance residual, Res, per half-hour interval was calculated from Eq. (1) as follows:

$$Res = R_N - LE - G - H - S \quad (3)$$

with LE from either EC or EC-LC ($\mathrm{LE_{EC}}$ and $\mathrm{LE_{EC-LC}}$, respectively) and H from EC.

2.2.3 Low-cost eddy covariance (EC-LC)

The EC-LC set-ups comprised of the same ultrasonic anemometer uSONIC3-omni as used for the EC and ECEB set-ups plus a compact low-cost relative humidity, air temperature and pressure sensor (BME280, BOSCH, Germany, Table 2). Water vapour mole fraction was calculated using measurements of relative humidity, air temperature and air pressure from the low-cost thermohygrometer. A derivation of the water vapour mole fraction from the low-cost thermohygrometer is given in Section A2. The turbulent water vapour fluxes were calculated as the covariance between the vertical wind velocity and the water vapour mole fraction from EC-LC, as per the principle of the eddy covariance method (Baldocchi, 2014). The cheaper but slower thermohygrometer had inferior spectral response characteristics compared to a gas analyser of fast response. The mean spectral correction factor of the thermohygrometer was 42% larger than for the LI-7200 fast response gas analyser for reference, with a 78% larger mean time constant of the thermohygrometer compared to the LI-7200. The mean time constant of the thermohygrometer and the LI-7200 was 2.8 ± 1 s and 0.6 ± 0.3 s, respectively (Markwitz and Siebicke, 2019). Spectral losses in the high-frequency range of the energy spectrum of the thermohygrometer were corrected by the fully analytical correction method of Moncrieff et al. (1997), which was explicitly recommended for either open-path sensors or closed-path sensors of heated and very short sampling lines. A detailed description and application of the EC-LC set-up for evapotranspiration measurements over AF and MC is given in Markwitz and Siebicke (2019). Evapotranspiration from EC-LC was neither gap-filled for the methodological comparison nor for the analysis of the energy balance closure due to the risk for new errors and artefacts from the respective gap-filling method.

2.3 Gap-filling and energy balance closure adjustment

For the comparison of $\mathrm{ET_{EC}}$, $\mathrm{ET_{ECEB}}$ and $\mathrm{ET_{EC-LC}}$ and the estimation of the energy balance closure during the campaigns, we neither gap-filled the data, nor corrected the data for the energy balance non-closure. For the calculation of annual sums of $\mathrm{ET_{ECEB}}$ and $\mathrm{ET_{EC-LC}}$ data gaps were filled, and corrected for the energy balance non-closure by distributing the residual equally to H and LE. The residual was estimated by machine learning for times when no data were available. In the following subsections we describe the gap-filling and energy balance closure adjustment procedures for the ECEB and EC-LC set-ups in more detail.

2.3.1 ECEB

For the calculation of annual sums of $\mathrm{ET_{ECEB}}$, gaps were filled with the online eddy covariance gap-filling and flux-partitioning tool REddyProc developed at the Max Planck Institute for Biogeochemistry in Jena, Germany (https://www.bgc-jena.mpg.de/bgi/index.php/Services/REddyProcWeb, last access: 19 January 2020). The methods used therein are based on Falge et al.

(2001) and Reichstein et al. (2005). We corrected $\mathrm{ET_{ECEB}}$ for the average energy balance non-closure, which we estimated from direct LE measurements by EC during measurement campaigns of minimum four weeks duration. In the current study we found that considering the energy balance residual reduces $\mathrm{ET_{ECEB}}$. We used machine learning to estimate the energy balance residuals (Eq. (3)) during times when no campaigns took place. We used the machine learning technique Extreme Gradient Boosting (Chen and Guestrin, 2016; Chen et al., 2019) and predicted the residual energy for both years, 2016 and 2017, at all sites with the R-package xgboost (Chen et al., 2019).

The calculated residual was treated as the dependent variable, whereas the net radiation, the ground heat flux and the sensible heat flux were treated as the independent variables. The model was tested with the data gathered during the campaigns and divided into a training period and a testing period. At a ratio of 2/3 of training to testing data, we achieved a Pearson correlation coefficient between the testing and predicted data of 0.66. The trained model was then applied to both years, with the net radiation, the ground heat flux and sensible heat flux as input parameters. As a last step the predicted residual was subtracted from half-hourly ET. We assumed that the residual distributes equally to the LE and H, thus subtracted only half of the residual from ET. Commonly, the residual energy is partitioned according to the Bowen ratio (Twine et al., 2000), which requires direct and continuous measurements of H and LE by EC. We decided for an equal separation of the residual energy because direct LE measurements by EC were not continuously available at our sites. This assumption may cause an overestimation of LE during dry ambient conditions, when the Bowen ratio is high. In contrast, LE is expected to be underestimated during moist ambient conditions, when the Bowen ratio is small. As no campaign on the energy balance closure was conducted at the monoculture system of Reiffenhausen, we used the data gathered during the campaign at the AF system of Reiffenhausen to train the model and to predict the residual at the MC system.

2.3.2 EC-LC

Unlike for the methodological comparison and energy balance analysis, a gap-filling of $\mathrm{ET_{EC-LC}}$ could not be avoided for the calculation of annual sums of ET. Therefore, for these analyses we gap-filled the half-hourly $\mathrm{ET_{EC-LC}}$ with half-hourly $\mathrm{ET_{ECEB}}$ and corrected both $\mathrm{ET_{EC-LC}}$ and $\mathrm{ET_{ECEB}}$ for the surface energy balance closure as follows

1. The residual energy was estimated from all available data in 2016 and 2017, following Eq. (3).

2. We used the calculated residual as the dependent variable and the net radiation, the ground heat flux and the sensible heat flux as independent variables to train the same machine learning tool as used for ECEB.

3. The residual was predicted by the trained model; data gaps in the residuals, originating mainly from missing LE caused by data quality checks, were filled with the predicted values.

4. Subsequently, we distributed the residual to $\mathrm{ET_{EC-LC}}$ ($\mathrm{LE^{cor}_{EC-LC}}$) and to $\mathrm{ET_{ECEB}}$ used for gap-filling ($\mathrm{LE^{gf}_{ECEB}}$) as follows.

$$\alpha = 0.5 \tag{4}$$

$$LE^{cor}_{EC-LC} = LE_{EC-LC} + Res \cdot \alpha \tag{5}$$

$$LE^{gf}_{ECEB} = LE^{gf}_{ECEB} - Res \cdot \alpha \tag{6}$$

2.4 Energy balance closure estimation

The energy balance closure (EBC) was quantified in two ways:

1. As the linear regression between the available energy (R_N - G - S), and the sum of the turbulent flux components (LE + H). We applied the major axis linear regression (Webster, 1997), which assumes equally distributed errors in both time series. We interpret the slope between the available energy and the sum of the turbulent fluxes as the closure of the surface energy balance. A slope of one and an intercept of zero corresponds to perfect energy balance closure. In the present study both the slope and the intercept were considered as variable.

2. As the energy-balance-ratio (EBR) or also called "instantaneous energy balance closure" (Stoy et al., 2013), thus the closure per half an hour:

$$EBR = \frac{LE + H}{R_N - G - S}, \tag{7}$$

with either $\mathrm{LE_{EC}}$ or $\mathrm{LE_{EC-LC}}$.

2.5 Flux footprint analysis

The spatial coverage and the position of the source area of turbulent sensible- and latent heat fluxes, and momentum at a specific point in time is defined by the flux footprint (Schmid, 2002; Kljun et al., 2015). In the present study a flux footprint climatology was calculated with the flux footprint prediction online data processing tool developed by Kljun et al. (2015) (http://footprint.kljun.net/, last access: 19 January 2020). The analyses were performed separately for the respective campaign periods (Table A1 for dates) and for both years at each site. We selected only daytime data, according to a global radiation $\mathrm{R}_G > 20\ \mathrm{W m^{-2}}$.

2.6 Canopy resistance

Effects of structural differences between AF and MC on ET were studied in terms of the relationship between half-hourly ET and the aerodynamic and canopy resistances ($\mathrm{s\,m^{-1}}$). The canopy resistance was calculated from the rearranged Penman-Monteith equation (Eq. (A12)) for evapotranspiration, which depends on the canopy resistance, $\mathrm{r_c} = 1/\mathrm{g_c}$ ($\mathrm{s\,m^{-1}}$), and the aerodynamic resistance for heat, $\mathrm{r_{ah}} = 1/\mathrm{g_{ah}}$ ($\mathrm{s\,m^{-1}}$). The canopy resistance follows the big leaf assumption, assuming that the whole canopy response to environmental changes equals the response of a single leaf. This assumption is valid for the monoculture system with a single crop type of similar height. For the AF systems this assumption might be violated due to the heterogeneity of the AF systems with different plant species (trees and crops) of different heights. In the lee of the tree strips the reduced wind speed and incident radiation might lead to reduced ET due to a different leaf stomata regulation of sunlit and shaded leafs. In the windward site of the tree strips trees and crops are affected by increased wind velocities and varying incident radiation, thus opposite conditions compared to the lee of the tree strips. However, we assume that the meteorological data from the flux tower represent the mean state of the meteorological conditions within the AF system. Therefore, we are confident that the big-leaf assumption also holds for AF systems.

We studied the relationship between ET and canopy resistance and aerodynamic resistance for idealized ambient conditions, with global radiation, $\mathrm{R_G} \geq 400\ \mathrm{W\,m^{-2}}$, horizontal wind speed, $\mathrm{u} \geq 1\mathrm{m\,s^{-1}}$ and vapour pressure deficit, $\mathrm{D} = 1 \pm 0.3\mathrm{kPa}$ (Schmidt-Walter et al., 2014). A derivation of the canopy resistance is given in Section A3.

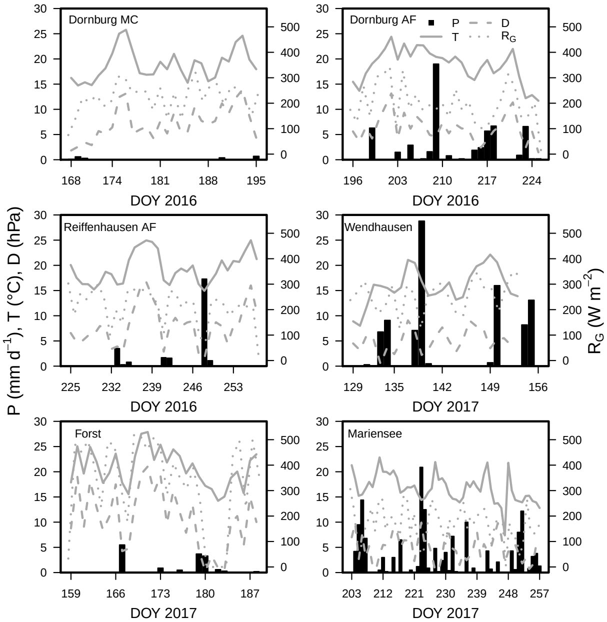

Figure 2. Time series of daily mean air temperature, T ($^{\circ}$C), vapour pressure deficit, D (hPa), daily summed precipitation ($\mathrm{mm\,d^{-1}}$) (left y-axis) and daily mean global radiation, R_G ($\mathrm{W\,m^{-2}}$), (right y-axis) for all sites. The data for AF and MC of the respective sites of Forst, Mariensee and Wendhausen were averaged. The field campaigns at the AF and MC systems were conducted during the same time and we assumed similar weather conditions due to the small distance between the AF and MC system.

3 Results and discussion

3.1 Meteorological conditions during the campaigns

For the meteorological conditions during the campaigns we refer to time series of relevant meteorological parameter in Figure 2 and mean values in Table 3.

3.2 Flux footprint climatology

The flux footprint analyses showed that the measured turbulent fluxes were representative for the larger AF systems and their respective MC systems during the time of the experiments (e.g. Dornburg, Forst and Wendhausen, Fig. 3). At the AF and MC systems of Dornburg 80 % of the flux magnitude originated from the respective system. The 90 % flux magnitude contribution line at the AF system overlapped with the 90 % flux magnitude contribution line at the MC system towards the west. The overlapping footprint was also found for the annual footprint analyses (Fig. A3).

At the AF and the MC system of Wendhausen we observed a 80 % flux magnitude contribution from both land-uses to the total turbulent flux (Fig. 3). A 10 % flux magnitude contribution originated from the forest around 200 m east of the flux tower.

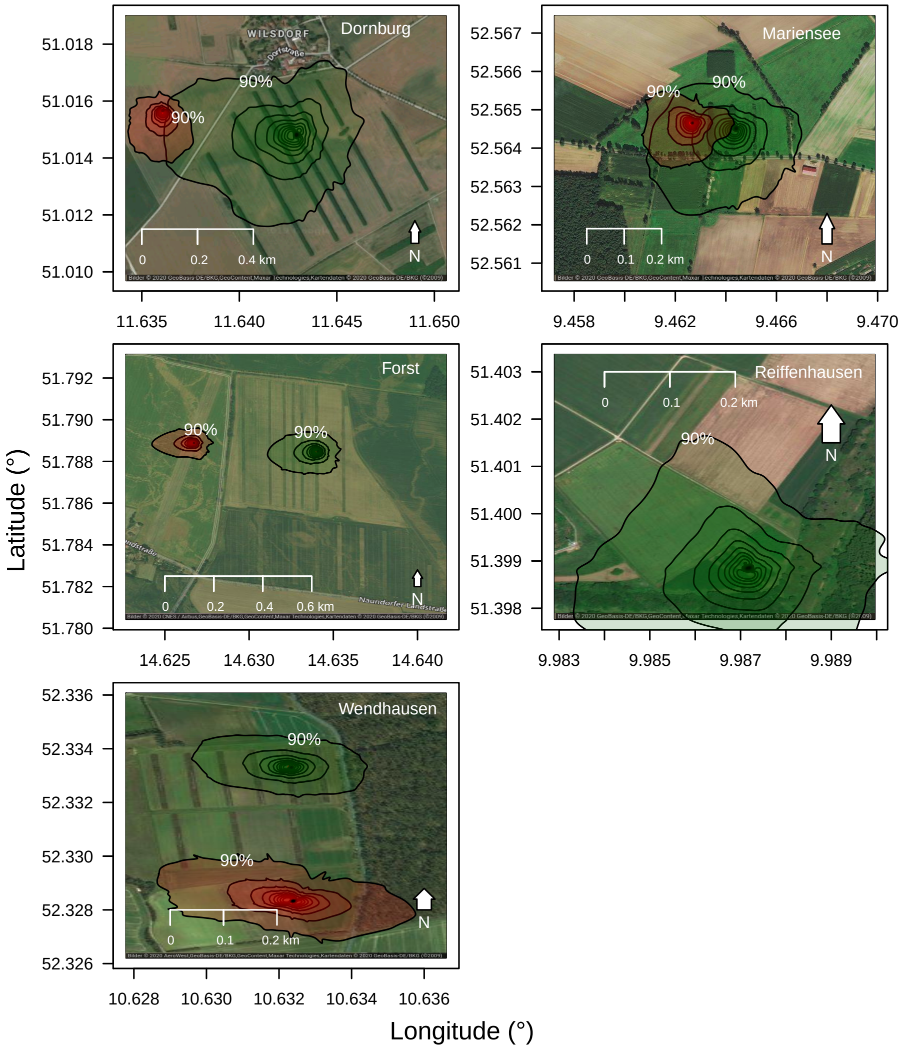

Figure 3. Flux footprint climatologies for all sites for the respective campaign period. Green shaded footprints correspond to the AF system and red shaded footprints correspond to the MC system. For the analysis only daytime data were used ($R_G > 20\ \mathrm{Wm}^{-2}$). Isolines correspond to a 10 to 90 % flux magnitude contribution in 10 % steps, with the 90 % isoline labelled in the system. The flux footprint climatology for Reiffenhausen MC is missing due to the unavailability of a campaign. Aerial photographs originate from Google maps/ Google earth ©Google 2020.

Table 3. Mean air temperature, T (°C), vapor pressure deficit, D (hPa), global radiation, R_G ($W\,m^{-2}$), and the cumulative precipitation, P ($mm\,d^{-1}$), for the respective site and campaign period. Data for Reiffenhausen MC are missing due to the unavailability of a campaign.

Site	T (°C)	P (mm)	D (hPa)	R_G (Wm^{-2})
Dornburg AF	19.0	57.1	6.41	200.7
Dornburg MC	18.6	2.1	7.35	212.6
Forst AF	21.4	18.9	12.02	358.8
Forst MC	21.2	14.8	11.88	371.5
Mariensee AF	18.54	40.6	6.2	258.9
Mariensee MC	16.93	163.5	4.7	172.8
Reiffenhausen AF	19.31	26.3	8.02	219.1
Wendhausen AF	16.6	48.6	5.4	235.0
Wendhausen MC	15.5	90.7	5.2	239.9

Easterly winds are most likely during stable atmospheric stratification in winter or summer. During the time of the experiment the wind mainly originated from westerly directions (not shown).

70 % of the area of the AF and MC grassland systems of Mariensee contributed to the measured fluxes, respectively (Fig. 3). The remaining 20 % of the area contributing to the measured flux originated from surrounding crops and the AF and MC grassland systems. There was an overlap of the two footprints at the AF and the MC grassland system, which was expected, as both flux towers are separated by a distance of about 200 m.

The fluxes measured at the smallest AF system in Reiffenhausen were influenced by fluxes originating from the nearby forests and crop fields about 400 m distance to the flux tower in northerly direction and about 200 m distance in southerly direction (Fig. 3). Only 60 % of the fluxes originated from the willow-grassland AF system and the short rotation willow plantation in the west. The terrain at the AF system of Reiffenhausen is sloped towards the north-west. The main wind direction at the site was north-northwest in the direction of the sloped terrain.

3.3 Diel evapotranspiration

The diel variation of ET for all three set-ups at all sites is depicted in time series plots for an exemplary time period in Figure 4.

The EC-LC set-up showed the best performance relative to direct EC measurements with coefficients of determination between minimum 71 % and maximum 94 %. The EC-LC set-up captured the temporal variability of ET and the flux response to changing ambient conditions as good as direct EC measurements. The slopes from a linear regression analysis of LE_{EC-LC} versus LE_{EC}, showed an agreement between 86 % and 99 % across four AF systems and between 108 % and 142 % across four monoculture agriculture systems (Table 4 and Fig. A2).

At the MC systems of Forst and Wendhausen (Fig. 4) we observed comparably high $\mathrm{ET_{EC-LC}}$ relative to direct EC measurements, while attaining high coefficients of determination. We suspect that the laser source of the LI-7200 gas analyser did not work as expected as indicated by spectral analysis (data not shown). Only low-frequency fluctuations were sampled, whereas the high-frequency fluctuations were attenuated. The spectral response characteristics of the gas analyser and the thermohygrometer set-up were similar. Therefore, the correction of high-frequency losses is expected to be higher for the compromised gas analyser at the respective MC systems, than for a fully functional gas analyser.

$\mathrm{ET_{ECEB}}$ also captured the diel cycle of ET and gave an indication on the ecosystem response to changing meteorological driver (Fig. 4). $\mathrm{ET_{ECEB}}$ overestimated $\mathrm{ET_{EC}}$ across all sites. A minimum overestimation of 27 % was observed at the AF system of Forst and a maximum overestimation of 101 % was observed at the MC system of Forst at half-hourly time scale (Table 4 and Fig. A1). Differences between $\mathrm{ET_{ECEB}}$ and $\mathrm{ET_{EC}}$ were attributed to the assumption of a fully closed energy balance at the surface (Foken et al., 2006). $\mathrm{ET_{ECEB}}$ was calculated as the residual of net radiation, sensible heat flux, ground heat flux and soil storage. In this analysis we did not account for the commonly observed non-closure of the energy balance and added the surface energy balance residual completely to LE.

3.4 Energy Balance Closure (EBC)

3.4.1 EBC from EC and EC-LC

The mean EBC was 79.4±8.5 % and 79.25±6 % across the five AF systems and four MC systems for $\mathrm{LE_{EC}}$ (Fig. 5 and Table 5). The coefficient of determination, R^2, was minimum 0.77 and maximum 0.92 across sites (Table 5).

The EBC for $\mathrm{LE_{EC}}$ at the AF and the MC systems were comparable to agricultural systems as reported by Stoy et al. (2013), who found a mean EBC of 84±20 % across 173 FLUXNET sites, a mean EBC of 91 % to 94 % for evergreen broadleaf forests and savannas and a mean EBC of 70 % to 78 % for crops, deciduous broadleaf forests, mixed forests and wetlands. Imukova et al. (2016) found an EBC of 71 % and 64 % for two consecutive growing seasons over a winter wheat stand in Germany. Studying a belt and alley system in Australia Ward et al. (2012) found an EBC between 67 % and 80 % over the time period of half a year. Fischer et al. (2018) reported on water requirements of three short rotation poplar stands and found a mean long-term energy balance closure of 82 % at a site in Italy, an EBC of 91 % or 95 % at a site in the Czech Republic and an EBC of 69 % at a site in Belgium.

The EBC for $\mathrm{LE_{EC-LC}}$ was slightly lower at the AF systems with a mean EBC of 79±5.3 % compared to the MC systems with a mean EBC of 82±11.8 % for five sites. The differentiation into lower EBC at the AF and higher EBC at MC systems observed for the two different set-ups is in agreement with the linear regression results presented in Section 3.3. At the AF systems $\mathrm{LE_{EC-LC}}$ was lower than $\mathrm{LE_{EC}}$. In the calculation of the energy balance closure only LE was changed and the other energy balance components were held constant. Therefore, increased LE led to a decreased residual energy and subsequently to a better fit of the energy balance closure.

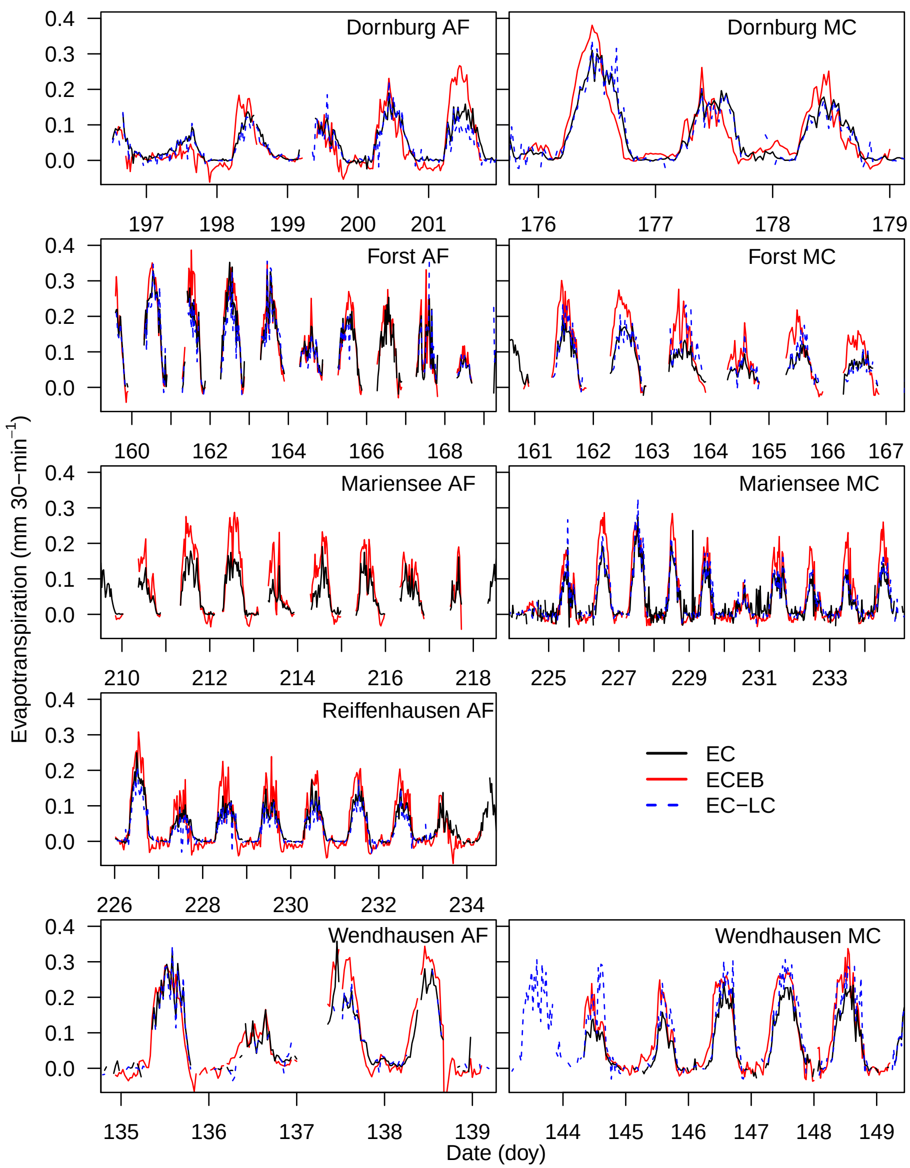

Figure 4. Time series of half-hourly evapotranspiration rates of an exemplary time period, for ECEB, EC-LC and EC as a reference for all sites. Time series of half-hourly ET rates for Reiffenhausen MC are missing due to the unavailability of a campaign and $\mathrm{ET_{EC-LC}}$ at Mariensee AF are missing due to technical problems of the sensor during the campaign. The presented time series were not corrected for the energy balance non-closure. Gaps in nocturnal data are due to the limited power availability from the solar power supply.

Table 4. Statistical analysis results for a linear regression of $\mathrm{LE_{EC-LC}}$ versus $\mathrm{LE_{EC}}$ and $\mathrm{LE_{ECEB}}$ versus $\mathrm{LE_{EC}}$. Shown are the root mean square error, RMSE, the standard deviation of the differences between both set-ups, SD, the bias, Bias, the number of points used for the analysis, n, the slope for a linear regression of $\mathrm{LE_{EC-LC}}$ versus $\mathrm{LE_{EC}}$ and $\mathrm{LE_{ECEB}}$ versus $\mathrm{LE_{EC}}$, and the coefficient of determination of the linear regression, $\mathrm{R^2}$. Data for $\mathrm{LE_{EC-LC}}$ at Mariensee AF are missing due to technical problems of the sensor during the campaign and data for Reiffenhausen MC are missing due to the unavailability of a campaign.

Sites	Method	RMSE ($\mathrm{Wm^{-2}}$)	SD ($\mathrm{Wm^{-2}}$)	Bias ($\mathrm{Wm^{-2}}$)	n	Slope	$\mathrm{R^2}$
Dornburg AF	ECEB/EC	67.65	67.33	-6.23	1202	1.93	0.45
	EC-LC/EC	35	31.93	-11.14	1037	0.94	0.71
Dornburg MC	ECEB/EC	71.53	71.51	2.31	1152	1.33	0.52
	EC-LC/EC	34.31	34.3	1.1	1030	1.08	0.86
Forst AF	ECEB/EC	58.91	57	7.64	549	1.27	0.79
	EC-LC/EC	38.5	36.74	-2.13	197	0.95	0.9
Forst MC	ECEB/EC	74.5	61.70	18.42	612	2.01	0.7
	EC-LC/EC	37.9	34.5	5.3	461	1.42	0.8
Mariensee AF	ECEB/EC	79.79	65.54	23.82	1503	2.0	0.78
	EC-LC/EC	–	–	–	–	–	–
Mariensee MC	ECEB/EC	61.1	59.81	8.81	1852	1.42	0.75
	EC-LC/EC	44.6	43.9	4.62	1520	1.16	0.8
Reiffenhausen AF	ECEB/EC	55.4	55.23	4.1	1395	1.65	0.74
	EC-LC/EC	27.84	23.61	-2.72	279	0.86	0.9
Wendhausen AF	ECEB/EC	68.30	67.88	5.34	954	1.3	0.8
	EC-LC/EC	33.5	32.7	-3.1	586	0.99	0.94
Wendhausen MC	ECEB/EC	73.42	61.14	24.4	792	1.41	0.85
	EC-LC/EC	57.9	47	15.53	604	1.3	0.89

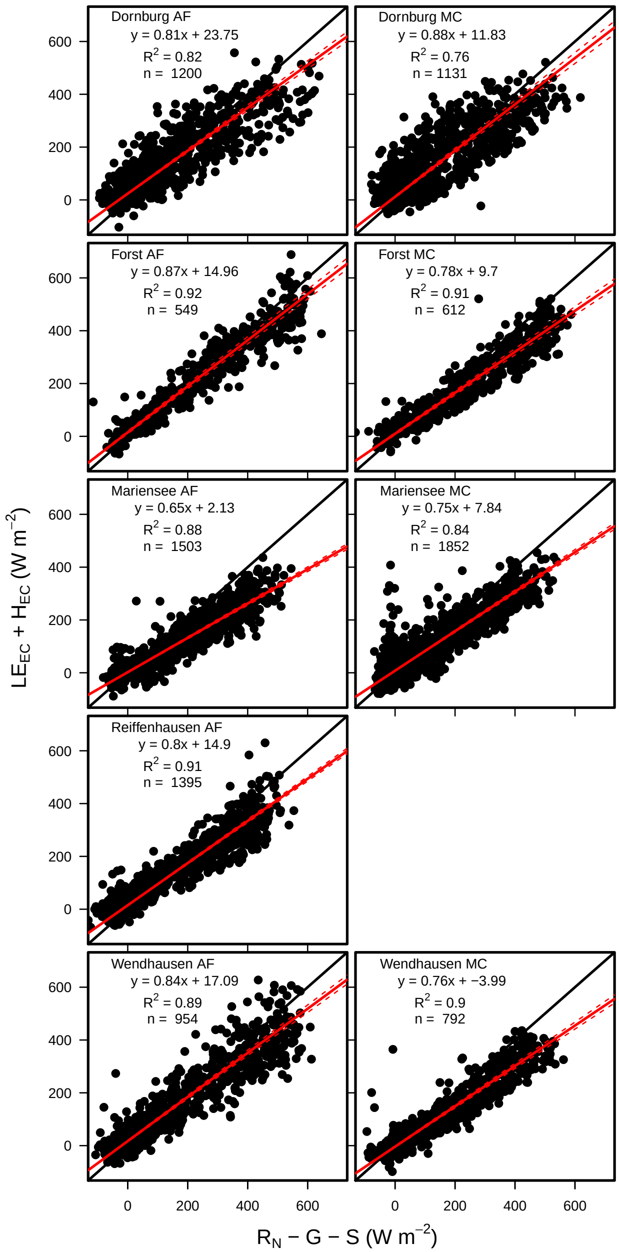

Figure 5. Scatterplot of the sum of the turbulent fluxes ($\mathrm{LE_{EC} + H_{EC}}$) versus the sum of the available energy ($\mathrm{R_N - G - S}$) for all sites. Each plot contains the linear regression equation, the coefficient of determination, $\mathrm{R^2}$, and the number of data points used for the analysis, n. Data for Reiffenhausen MC are missing due to the unavailability of a campaign.

Table 5. Statistical analysis results of the linear regression between the sum of the turbulent fluxes and the available energy. Namely, the sites, the set-up used, the slope (±5 % confidence interval), intercept, the coefficient of determination of the linear regression, R^2, and the number of points used for the analysis, n. The energy balance closure determined by EC-LC at Mariensee AF is based on data collected from 23 March 2016 to 20 November 2016 and at Reiffenhausen MC the analyses are based on data collected from 07 April 2016 to 31 December 2016, due to the unavailability of data during the campaigns. The energy balance closure determined by EC for Reiffenhausen MC is missing due to the unavailability of a campaign.

Sites	Set-up	Slope	Intercept (Wm^{-2})	R^2	n
Dornburg AF	EC	0.81± 0.02	23.75±1.95	0.82	1200
	EC-LC	0.75± 0.03	17.3±2.6	0.72	1088
Dornburg MC	EC	0.88± 0.025	11.83±3.1	0.76	1131
	EC-LC	0.90± 0.035	12.03±4.2	0.70	1046
Forst AF	EC	0.87± 0.02	14.96±5.1	0.92	549
	EC-LC	0.81± 0.045	17.2 ±11.1	0.85	205
Forst MC	EC	0.78± 0.02	9.7±4.4	0.91	612
	EC-LC	0.85± 0.03	10.3±7.9	0.85	486
Mariensee AF	EC	0.65± 0.01	2.13±1.63	0.88	1503
	EC-LC	0.85± 0.009	-1±0.6	0.85	6525
Mariensee MC	EC	0.75± 0.015	7.8±1.2	0.84	1852
	EC-LC	0.82± 0.015	7.7±1.4	0.88	1632
Reiffenhausen AF	EC	0.80± 0.01	14.94±1.2	0.91	1395
	EC-LC	0.72± 0.03	10.55±3.1	0.91	306
Reiffenhausen MC	EC	–	–	–	–
	EC-LC	0.62± 0.005	5.7±0.35	0.84	9717
Wendhausen AF	EC	0.84± 0.02	17.1±2.8	0.89	954
	EC-LC	0.82± 0.03	13.8±4.4	0.84	641
Wendhausen MC	EC	0.76± 0.02	-3.9±2.6	0.9	792
	EC-LC	0.91± 0.025	3.1±4.4	0.85	710

3.4.2 Diel cycles of the energy balance ratio and the energy balance residual

The diel cycle of the energy balance ratio from $\mathrm{LE_{EC}}$ at the sites can be classified into two different patterns. The diel cycle of the EBR for Dornburg (Fig. 6) show a strong increase between 6 am and 8 am, followed by a positive slope between 8 am and 2 pm, and a strong increase thereafter until 6 pm. The EBR is minimum 0 at 6 am and maximum 1.8 at 6 pm. The diel cycle of the EBR at the remaining sites (Forst, Mariensee, Reiffenhausen and Wendhausen, Fig. 6) is lowest at 6 am and 6 pm with an EBR of 0.5, whereas between 8 am and 4 pm the EBR is fairly constant at a similar range as the EBC estimated for all sites and the whole campaign (Table 5).

The Dornburg site might be affected by horizontal advection of moisture and heat. Oncley et al. (2007) reported that the advection of moisture had the highest contribution to the unclosed energy balance compared to the other components. The maximum peak of the horizontal moisture advection term was in the afternoon, as energy was accumulated during the day and released in the afternoon. We suspect that this is also the case for the Dornburg site. The sensible heat flux follows the diurnal cycle of available energy with the maximum peak at midday at the agroforestry and the monoculture system (Fig. 7). In contrast, the median of the latent heat flux had its maximum in the afternoon at around 2 pm and was positive even after the available energy changed its sign.

In addition to advective transport, the unclosed surface energy balance could be related to energy storage terms such as biomass, the air or photosynthesis (Jacobs et al., 2008), that have previously not been considered. The pattern seen at Dornburg may be attributed to a release of energy during the afternoon, which correspond to a surplus of energy and a better closure of the energy balance. In the morning hours the storage terms have an opposite sign, which correspond to a lack of energy and a subsequent poorer energy balance closure. Considering the storage terms would lead to a reduction of the residual energy and a better closure of the energy balance.

Interestingly, the diel pattern of the EBR from $\mathrm{LE_{EC}}$ at both land-uses at all sites are equal. Additionally, the differences between the median diel cycle EBRs (between 6 am and 6 pm) at the AF and the MC system were small, with differences of minimum -0.09 and maximum 0.13 across sites. As both flux towers located at the AF and the MC system at one site are separated by approximately 100 to 500 m and the diel patterns look similar, we suspect that the non-closed surface energy balance at one site is caused by local effects of longer wavelength than the commonly applied averaging period of 30 minutes and beyond the individual site level.

The diel cycles of the EBRs and the residuals were similar for both EC-LC and EC set-ups (Fig. A4). This is promising, as it indicates first, a performance of EC-LC comparable to EC, and, second, the capability of the EC-LC set-up to capture site-specific effects. Nevertheless, the observed differences between EBRs and residuals at the AF and MC at one site were mostly attributed to differences in LE. Higher $\mathrm{LE_{EC-LC}}$ than $\mathrm{LE_{EC}}$ led to higher EBRs.

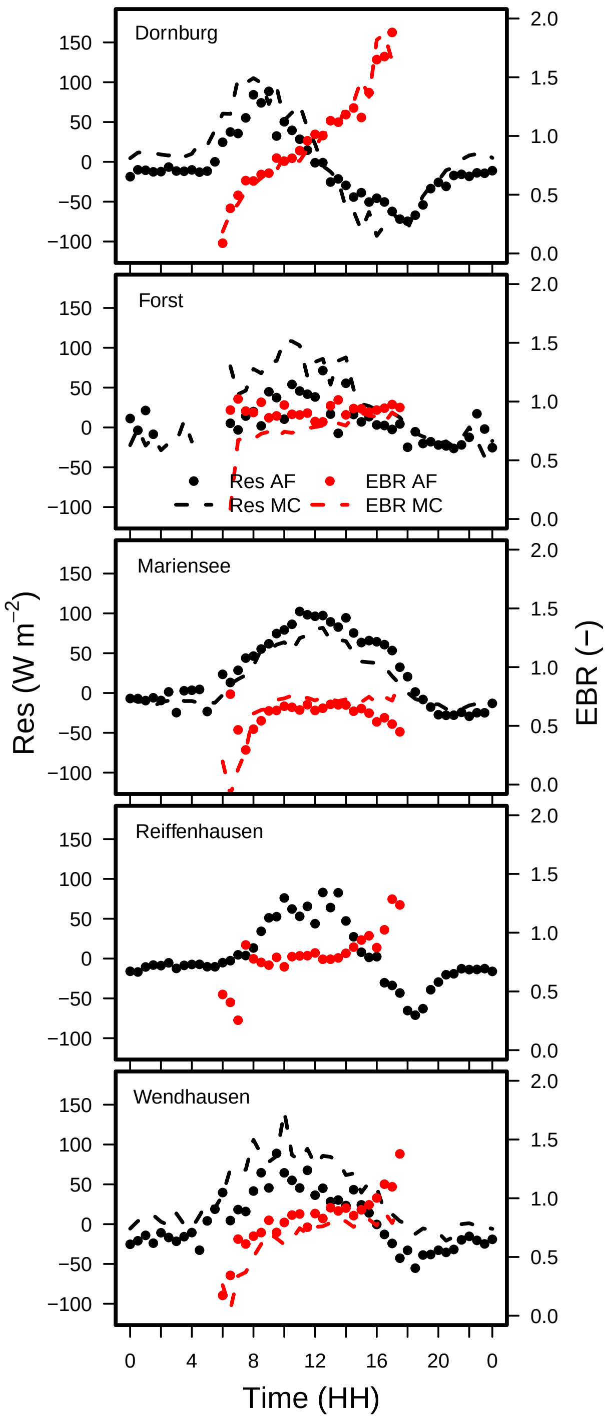

Figure 6. Median diel cycle of the energy balance ratio (EBR) and diurnal cycle of the residual energy for the AF and the MC systems at all sites. LE and H were obtained by EC. Data from Reiffenhausen MC are missing due to the unavailability of a campaign.

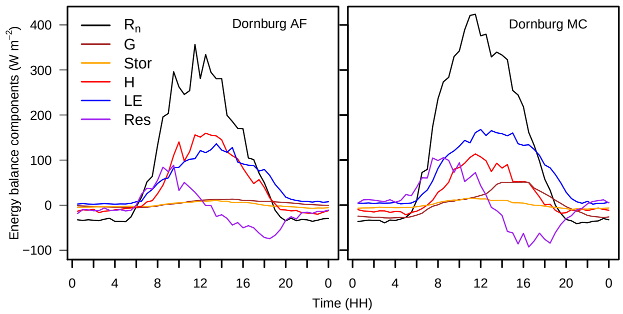

Figure 7. Median diurnal cycle of the energy balance components for Dornburg AF and MC for the campaign times (Table A1).

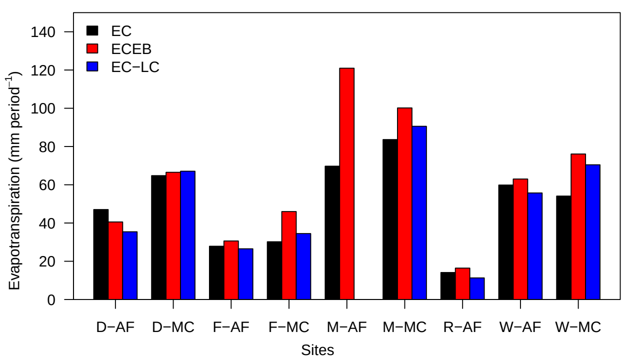

Figure 8. Sums of uncorrected and not gap-filled half-hourly evapotranspiration for all three methods and all sites during the campaign periods. Sites are abbreviated by their first letter and contain either AF for agroforestry or MC for monoculture. Incomplete records with either $\mathrm{ET_{EC}}$, $\mathrm{ET_{ECEB}}$ or $\mathrm{ET_{EC-LC}}$ missing were omitted. Data for $\mathrm{ET_{EC-LC}}$ at Mariensee AF are missing due to technical problems of the sensor during the campaign and all data for Reiffenhausen MC are missing due to the unavailability of a campaign.

3.5 Evapotranspiration over agroforestry

3.5.1 Sums of evapotranspiration during the campaigns

Sums of evapotranspiration for all three methods, all sites and the campaign periods indicate higher sums of $\mathrm{ET_{ECEB}}$ relative to $\mathrm{ET_{EC}}$, except for Dornburg AF (Fig. 8). The difference between sums of $\mathrm{ET_{ECEB}}$ and $\mathrm{ET_{EC}}$ reflect the unaccounted correction of $\mathrm{ET_{EC}}$ and $\mathrm{ET_{ECEB}}$ for the energy balance non-closure. The large difference between sums of $\mathrm{ET_{ECEB}}$ and $\mathrm{ET_{EC}}$ at Mariensee AF correspond to the low energy balance closure of 65 % at the site. Differences between sums of $\mathrm{ET_{EC-LC}}$ and $\mathrm{ET_{EC}}$ correspond to lower $\mathrm{ET_{EC-LC}}$ than $\mathrm{ET_{EC}}$ over the AF systems and higher $\mathrm{ET_{EC-LC}}$ than $\mathrm{ET_{EC}}$ over the MC systems. This is indicated by slopes smaller and higher one of a linear regression analysis between $\mathrm{ET_{EC-LC}}$ and $\mathrm{ET_{EC}}$ (Table 4).

3.5.2 Weekly sums of evapotranspiration

The annual cycle of evapotranspiration across all sites and for the years, 2016 and 2017, depict the typical seasonal cycle of highest ET during summer and lowest ET during winter (Fig. 9). We found small differences between weekly sums of ET at the AF and the MC systems during the main growing period of the crops. After ripening of the crops, we found higher weekly sums of ET at the AF systems compared to the MC systems at the cropland sites of Dornburg, Forst and Wendhausen (Fig. 9). We assume that after the ripening of the crops evaporation contributed the most to the measured ET at the MC system, whereas at the AF system both evaporation from the crop fields between the tree strips and transpiration from the trees contributed to the measured flux. At the grassland sites of Mariensee and Reiffenhausen (Fig. 9) differences in weekly sums of ET between both land-uses were small with a tendency of higher ET rates at the MC system compared to the AF system.

3.5.3 Annual sums of evapotranspiration

Differences between annual sums of ET for the two land-uses, AF and MC, were in the range of maximum +31 % and minimum -16 % (Fig. 10 and Table 6) across sites and methods. We wanted to understand where differences between annual sums of ET come from. Therefore, we investigated differences between ET according to 1) the effect of the different land-uses, AF and MC, 2) the effect of different methods, EC-LC and ECEB, and 3) the effect of different years, 2016 and 2017, with different precipitation inputs. For this purpose we used the relationship between the evapotranspiration index ($\sum$ET/$\sum$P) and the radiative dryness index ($R_n/\lambda P$) proposed by Budyko (Budyko, 1974). Figure 11 (a) shows the ET index as a function of the radiative dryness index for all sites, both set-ups and both years.

The figure indicates first that plots with an ET index larger than one were water limited, corresponding to an radiative dryness index $R_n/\lambda P>1$. Secondly, the figure shows a separation of the sites with an energy limitation ($R_n/\lambda P<1$) and water limitation ($R_n/\lambda P>1$) for the years 2016 and 2017, respectively.

With regards to the first finding, in 2016 the grassland sites Mariensee AF and MC, and Reiffenhausen AF had an ET index larger than one. At those sites, the annual sum of ET was generally high relative to the annual sum of precipitation (Fig. A5 c). This finding seems to be typical for grasslands. Williams et al. (2012) reported on average 9 % higher transformation of precipitation into evapotranspiration of grasslands compared to forests across 167 sites as part of the global FLUXNET flux measurement network. They concluded, first, that higher ET of grasslands may have been caused by the less conservative water use compared to trees and, second, that it could indicate that grasses have an extensive, well developed rooting system, similar to trees. Nevertheless, considering the water balance equation with precipitation equalling the sum of evapotranspiration and water runoff, an ET index larger than one indicates water losses via ET and no runoff. An ET index larger than one is only to be expected under ground water access, irrigation or the impact of a nearby stream. At the grassland site of Mariensee it is likely that the trees and grasses had ground water access, as the ground water table was at about 1.5-2 m depth.

The AF system in Reiffenhausen is located on a gentle slope with no ground water access, which we expect should promote run-off, contrary to the high ET index observed. But, the ET measurements are affected by a poplar and willow SRC in the south-southeast and north-northwest directly within the flux footprint (Section 3.2 and Fig. 3). And with respect to the overall

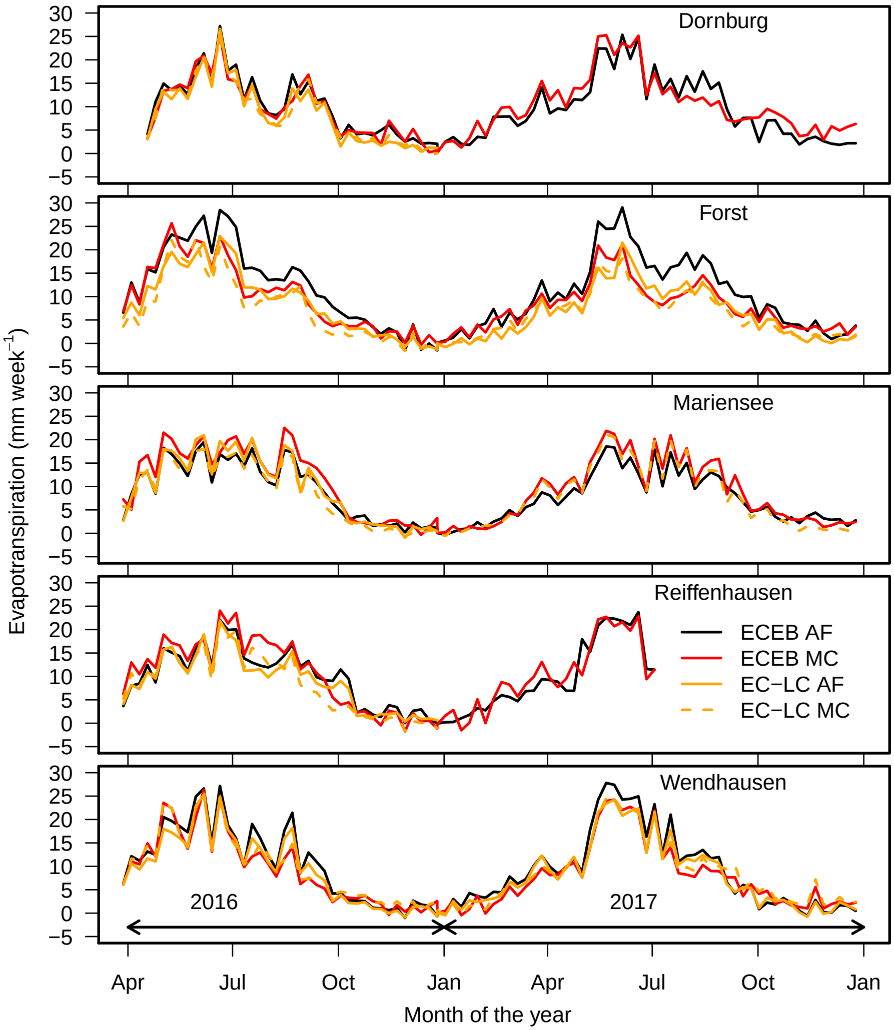

Figure 9. Weekly sum of half-hourly $\mathrm{ET}_{\mathrm{ECEB}}$ (black and red solid lines for AF and MC, respectively) and $\mathrm{ET}_{\mathrm{EC-LC}}$ (orange solid and dashed line for AF and MC, respectively) for all sites. In 2017 data in Reiffenhausen AF and MC were only available until the end of July due to station failure.

area of the AF system, the area covered by trees amounts to 72 % and is much higher, compared to the other sites (Table 1). In both cases, a radiative dryness index larger than one is also possible, despite this indicating a water limitation at the particular sites. Additionally this also indicates a surplus of radiative energy, which promotes photosynthesis and higher transpiration, if water is not limited. In contrast, the Mariensee and Wendhausen sites had evapotranspiration and radiative dryness indices of approximately 0.5 and 0.6 in 2017. Those sites were affected by exceptionally high annual precipitation events, but annual sums of ET comparable to 2016 (Table 6).

The second finding gives evidence for a dependency of ET on the local climate. The years 2016 and 2017 correspond to a dry and a wet year, respectively. In Figure 11 (a) and (b), arrows indicate the difference between mean evapotranspiraion indices and mean radiative dryness indices grouped by year, method and land-use. The length of the arrows correspond to the overall difference. The ET index averaged over all annual sums of ET for the years 2016 and 2017 showed the largest difference, with a trend from a water limited (2016) regime to an energy limited (2017) regime. Higher available energy and lower precipitation than normal in 2016 led to a higher radiative dryness index, whereas lower available energy and higher precipitation led to a smaller radiative dryness index in 2017. Differences between mean ET indices from the two methods had the second largest impact on annual sums, with a trend of a higher mean ET index of $\mathrm{ET_{ECEB}}$ compared to $\mathrm{ET_{EC-LC}}$. Land-use type had the least impact on differences between the ET indices, with a small trend of higher ET/P over AF than over MC.

However, our results indicate that the effect of agroforestry on ET is small compared to differences between methods and differences between years with different precipitation regimes. We therefore reject the initial hypothesis that short rotation alley cropping agroforestry systems lead to higher water losses to the atmosphere via ET, compared to monoculture agriculture without trees.

3.5.4 Effect of agroforestry on ET as explained by aerodynamic and canopy resistance

We wanted to understand if the heterogeneity of the AF systems can explain differences between half-hourly ET rates from AF relative to MC systems. We quantified the effect of surface heterogeneity on ET as per the relationship between half-hourly ET rates and aerodynamic and canopy resistances. Tree strips orientated perpendicular to the prevailing wind direction significantly reduce the wind speed (Böhm et al., 2014) and the aerodynamic resistance (Lindroth, 1993). The canopy resistance depends linearly on the aerodynamic resistance and is part of the first term of Eq. (A14). If the first term on the right hand side of Eq. (A14) is high, the canopy resistance is high and evapotranspiration is controlled by atmospheric processes. Whereas if the aerodynamic resistance is low the second term on the right hand side of Eq. (A14) dominates, i.e., ET is mainly controlled by the plants physiology.

Mean aerodynamic resistances, r_{ah}, were lower at the AF systems compared to the MC systems (Fig. 12). We interpret this as an effect of the higher roughness incurred by the higher tree alleys compared to the MC system. As an example we derived an aerodynamic resistance for two different canopy heights of 1 m and 5 m. We assumed a constant wind speed, u = 2 $\mathrm{m\,s^{-1}}$, universal constants for momentum ψ_m = 0.9 and heat ψ_h = 0.4, a measurement height z of 10 m and a displacement height d of 0.7 m and 3.5 m for a canopy height of 1 m and 5 m, respectively. We derived a roughness length for momentum and heat of 0.1 and 0.01 m for a canopy height of 1 m and of 0.5 m and 0.05 m for a canopy height of 5 m. Subsequently, we arrived at

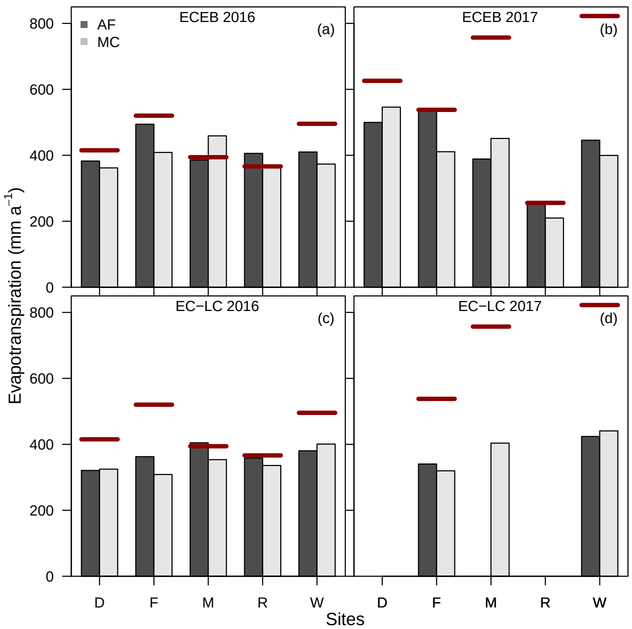

Figure 10. Annual sums of $\mathrm{ET_{ECEB}}$ in 2016, a, and 2017, b, and $\mathrm{ET_{EC-LC}}$ in 2016, c, and 2017, d, for Dornburg, "D", Forst, "F", Mariensee, "M", Reiffenhausen, "R", and Wendhausen, "W". The red solid lines correspond to the annual sum of precipitation from the monoculture system of the respective site. The annual sums of evapotranspiration at Reiffenhausen AF and Reiffenhausen MC in 2017 contain only data from 01 January 2017 to 09 July 2017 due to station failure. Annual sums of $\mathrm{ET_{EC-LC}}$ for Dornburg AF and MC, Mariensee AF, Reiffenhausen AF and MC in 2017 are missing due to instrument malfunctions.

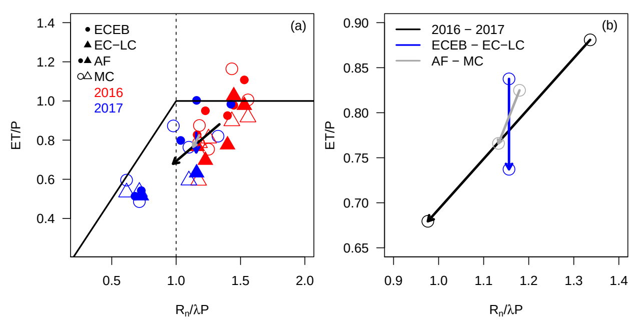

Figure 11. (a) Evapotranspiration index (ET/P) versus the radiative dryness index ($\mathrm{R}_n/\lambda\mathrm{P}$) for both land-uses (AF: filled triangles and dots; MC: empty triangles and dots), both set-ups (ECEB: dots; EC-LC: triangles) and both years (2016: red; 2017: blue). The bold black line describe regions of an energy limitation ($\mathrm{R}_n/\lambda\mathrm{P}<1$) and a water limitation ($\mathrm{R}_n/\lambda\mathrm{P}>1$). The arrows indicate mean trends of ET for the effect of different years (black arrow), different methods (blue arrow) and different land-uses (grey arrow). **(b)** Trends of the mean evapotranspiration index (ET/P) versus the mean radiative dryness index ($\mathrm{R}_n/\lambda\mathrm{P}$) for the effect of different years (black), different methods (blue) and different land-uses (grey) extracted from figure (a).

Table 6. Annual sums of energy balance closure corrected actual evapotranspiration, ET ($\mathrm{mm\,a^{-1}}$), and precipitation, P ($\mathrm{mm\,a^{-1}}$) for all sites, both set-ups (ECEB and EC-LC) and both years (2016 from April to December, and 2017 from January to December). The annual sums of $\mathrm{ET_{ECEB}}$ and precipitation at Reiffenhausen AF and MC in 2017 contain data from 01 January 2017 to 01 July 2017 due to destruction of the station. Annual sums of $\mathrm{ET_{EC-LC}}$ for Dornburg AF and MC, Mariensee AF, Reiffenhausen AF and MC in 2017 are missing due to instrument malfunctions.

Method	ECEB		EC-LC			
Sites	ET 2016	ET 2017	ET 2016	ET 2017	P 2016	P 2017
Dornburg AF	383	500	321	–	414	626
Dornburg MC	362	546	325	–	414	626
Forst AF	494	540	363	340	520	538
Forst MC	409	411	309	320	520	538
Mariensee AF	386	389	405	–	394	757
Mariensee MC	459	451	354	404	394	757
Reiffenhausen AF	406	252	358	–	366	256
Reiffenhausen MC	368	210	336	–	366	256
Wendhausen AF	410	446	380	424	496	822
Wendhausen MC	373	400	401	440	496	822

an aerodynamic resistance of 41.5 $\mathrm{s\,m^{-1}}$ for a canopy height of 1 m and of 10.3 $\mathrm{s\,m^{-1}}$ for a canopy height of 5 m. Thus, an increase in canopy height of 4 m led to a decrease in aerodynamic resistance of 75.2 %.

The relationship between half-hourly evapotranspiration rates and the canopy resistance at the sites followed an exponential function (Fig. 12). The differences between the mean canopy resistances at the AF and the MC systems were much smaller than differences in mean aerodynamic resistances at the AF and the MC systems. This suggests that the AF and the MC systems behave in a similar way from a plant physiological point of view, regarding the stomatal control of both the trees and the crops.

In the current study differences between annual sums of ET over AF and MC were small. Effects of AF on evapotranspiration rates are mostly attributed to a small region next to the tree strips (Kanzler et al., 2018), the quiet zone. There, the reduction of wind velocity and incident radiation is strongest and this causes a reduction of evapotranspiration. The quiet zone extends to roughly 4 to 12 times the tree height (Nuberg, 1998). The quiet zone changes to the wake zone, where the wind velocity increases and light is no longer limited, hence, evapotranspiration increases towards the centre between tree strips (Kanzler et al., 2018). As a result, lower ET in the quiet zone and higher ET in the wake zone might compensate each other on system-scale, leading to ET over AF comparable to ET over MC. A similar effect occurs when ET is measured over a whole AF system with e.g. the EC method (Baldocchi, 2003). EC measurements integrate over a larger area and small scale differences in between tree strips can not be detected.

3.6 Uncertainty and limitations of ET measurements over AF

As outlined in the previous section, differences in annual sums of ET between the different land-uses were small. Besides the discussed ecological reasons, we are aware of measurement errors due to the heterogeneous terrain (Foken, 2008b). The most critical assumptions of the eddy covariance method are horizontally homogeneous terrain and steady state ambient conditions (Foken et al., 2006; Foken, 2008b). It is assumed that the heterogeneities generate turbulent motions of longer time scale than the commonly applied averaging period of half an hour. This is also strongly connected to horizontal advection, commonly not properly represented in eddy covariance flux measurements. Foken et al. (2006) noted that the eddy covariance method is the most accurate method with errors between 5 and 10 %, depending on the turbulent conditions. The errors are higher during nighttime, due to limited turbulent conditions, causing a common flux underestimation (Aubinet et al., 2010). But during night especially ET is small and the effect of high errors are small, compared to daytime conditions when ET is high.

For the low-cost eddy covariance set-up we anticipate higher errors compared to direct EC, due to the limited time response of the thermohygrometer and subsequently higher spectral correction factors (Markwitz and Siebicke, 2019). We found that the effect of heterogeneity on ET is less important for EC-LC than the effect of different measurement heights (Markwitz and Siebicke, 2019). For a measurement height of 3.5 m, we found a latent heat flux underestimation compared to direct EC, and for a measurement height of 10 m, we found a slight latent heat flux overestimation (Table 4). At lower height the contribution of small and high-frequency fluctuations to the energy spectrum is higher. Due to the limited time response of the thermohygrometer between 1.9 and 3.5 seconds (Markwitz and Siebicke, 2019), the high-frequency eddies can not be adequately detected and the signal losses are higher.

In contrast, $\mathrm{ET_{ECEB}}$ might be affected by greater errors than $\mathrm{ET_{EC-LC}}$, due to multiple error sources inferred from each of the energy balance components, the assumption of a fully closed energy balance and resulting inaccuracies from the energy balance residual partitioning. For the ECEB set-up the heterogeneity of the landscape has a larger impact than for the EC-LC set-up, such as net radiation and ground heat flux measurements are not representative for the whole landscape.

Although errors for ET measurements with the respective set-ups can be large on a half-hourly time scale, for annual sums of ET, the errors often compensate each other and are small relative to the measured signal (Hollinger and Richardson, 2005). As an example, we calculated the random error uncertainty after Hollinger and Richardson (2005) for latent heat fluxes from Dornburg AF for 2016. The larger the integration time (hourly, daily and monthly), the smaller the random error. The magnitude of the random error was about 2.3 % (median over n = 9) of the flux magnitude for monthly averages, 11.55 % (n = 254) for daily averages and 34.5 % (n = 12191) for hourly averages. Hence, the random error for annual sums would be even smaller.

4 Conclusions

The main objective of the current work was to investigate the effect of AF on evapotranspiration in comparison to monoculture agriculture without trees. We performed evapotranspiration measurements at multiple sites, for two consecutive years by a low-cost eddy covariance set-up and an eddy covariance energy balance set-up.

In the first part of this paper we investigated the performance of the measurement set-ups. In comparison with direct eddy covariance measurements the low-cost eddy covariance set-up captured the temporal variability in half-hourly ET rates with high coefficients of determination during a comparison measuring campaign. The ECEB set-up also represented the diel cycle of ET, but was characterized by more scatter. We therefore conclude that the EC-LC set-up is a viable alternative compared to conventional eddy covariance set-ups, as the set-up represents ET of the underlying ecosystem more accurately than the ECEB set-up.

In the second part of paper work we focused on the question if AF systems have higher water losses to the atmosphere via ET compared to monoculture systems. Our results showed that differences in ET between AF and MC were small. Instead, we found higher evapotranspiration indices during a drier than normal year compared to a wet year across sites and methods. This shows that the potentially small effect from the trees on ET was overlaid by the effect of local climatic conditions. In addition, we found a similar plant physiological response of the AF and the MC systems, characterized by small differences between canopy resistances.

Overall, we conclude that the inclusion of tree strips into the agricultural landscape has not resulted in higher water losses to the atmosphere via ET and agroforestry can be a land-use alternative to monoculture agriculture without trees.

Data availability. All data used for the figures in this manuscript will be provided after final acceptance for publication.

Author contributions. CM designed and performed the field work, analysed the data and has written the current manuscript. AK and LS wrote the project scientific proposal, acquired the funding as part of the BonaRes SIGNAL consortium, and contributed to field work and analysis. All authors contributed to the discussion and manuscript writing.

Competing interests. The authors declare no competing interests.

Acknowledgements. We kindly acknowledge the funding from the German Federal Ministry of Education and Research (BMBF, project BonaRes, Modul A: Signal 031A562A) and from the Deutsche Forschungsgemeinschaft (INST 186/1118-1 FUGG). We further wish to acknowledge contributions by M. Herbst to the BonaRes SIGNAL proposal and project design and the technical support of field work received by F. Tiedemann, E. Tunsch, D. Fellert, M. Lindenberg, J. Peters (bioclimatology group) and D. Böttger (soil science group of tropical and subtropical ecosystems) from the University of Göttingen.

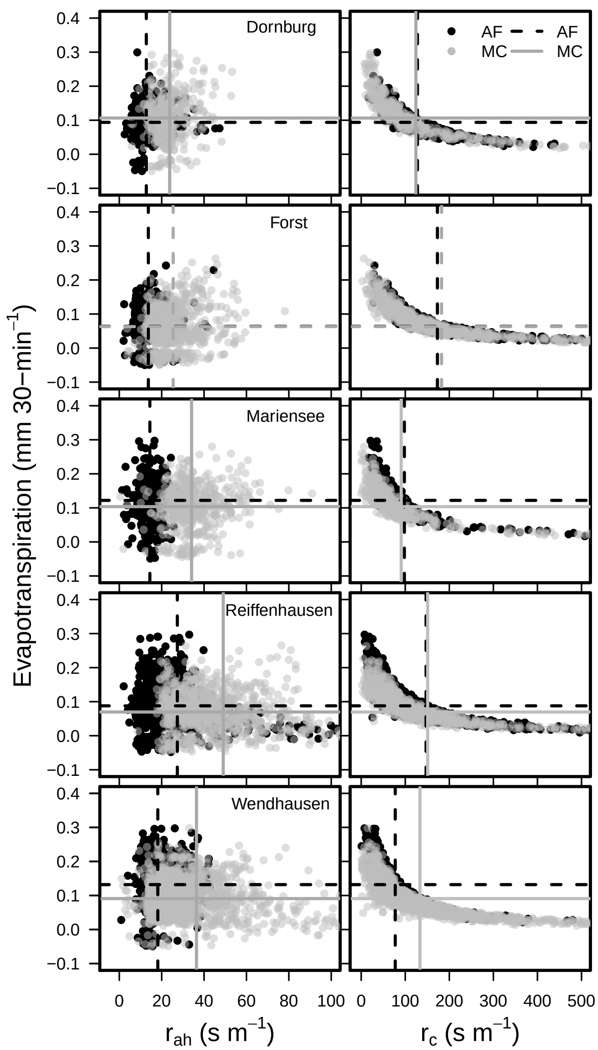

Figure 12. Half-hourly $\mathrm{ET_{EC-LC}}$ versus aerodynamic resistance, r_{ah} (left), and canopy resistance, r_c (right), for all sites. The dashed grey line corresponds to the mean aerodynamic and canopy resistance and evapotranspiration at the AF system and the dashed black line corresponds to the mean aerodynamic and canopy resistance and evapotranspiration at the MC system at the specific site. Only data corresponding to ideal ambient conditions are shown, e.g. a global radiation, $\mathrm{R}_G \geq 400\ \mathrm{W\,m^{-2}}$, a wind speed, u $\geq 1\ \mathrm{m\,s^{-1}}$ and a vapour pressure deficit, D = 1±0.3 kPa (Schmidt-Walter et al., 2014).

Appendix A: Derivations

A1 Half-hourly ET rates and soil storage flux

Half-hourly evapotranspiration rates in units of $\mathrm{mm\,30\,min^{-1}}$ were calculated from LE as

$$ET = \frac{LE_{ECEB}(\mathrm{J\,kg^{-1}\,s^{-1}})}{L(\mathrm{J\,kg^{-1}})} \cdot 1800(\mathrm{s\,30\,min^{-1}}) \cdot \frac{1}{\rho_{H_2O}}(\mathrm{m^3\,kg^{-1}}) \cdot 1000\,\mathrm{mm\,m^{-1}} \tag{A1}$$

with L ($\mathrm{J\,kg^{-1}}$) the latent heat of vaporization (Dake, 1972) depending on air temperature T ($^\circ\mathrm{C}$)

$$L = (2.501 - 0.00237T) \cdot 10^6, \tag{A2}$$

and $\rho_{\mathrm{H_2O}} = 1000\,\mathrm{kg\,m^{-3}}$ the density of liquid water.

The soil heat storage term has a major contribution to the unclosed energy balance (Foken, 2008a) and the magnitude of the soil heat storage is comparably larger than the other storage terms, i.e. the photosynthesis flux, the crop enthalpy change, the air enthalpy change, the canopy dew water enthalpy change and the atmospheric moisture change (Jacobs et al., 2008). We used the ground heat flux, G, from the ground heat flux measurements, $\mathrm{G_{HFP}}$ ($\mathrm{Wm^{-2}}$), at the sites and calculated the soil heat storage between the soil heat flux plate and the soil layer above following Liebethal and Foken (2007) as

$$G = G_{HFP} + \int\limits_{z=-0.05\,m}^{0\,m} c_v \frac{\partial T}{\partial t} dz \tag{A3}$$

The soil heat storage (second term on the right hand side of Eq. (A3)) consists of the vertical integral of the change of temperature over time at depth z = 0.02 m. c_v is the volumetric heat capacity of the soil, calculated from the soil components, i.e. organic, mineral and water and their respective heat capacities. Soil texture and bulk densities are summarized in Table A2 and were provided by Göbel et al. (2018) and Marcus Schmidt (pers. comm., Georg August University of Goettingen, Buesgen Institute, Soil Science of Tropical and Subtropical Ecosystems). Gaps in soil storage data were filled according to a multiple linear regression with soil storage versus net radiation and ground heat flux. The multiple linear regression fitting parameter were derived from records when the soil storage, the net radiation and the ground heat flux were available at the same time.

A2 Water vapour mole fraction $\mathrm{C_{H_2O_v}}$ from the thermohygrometer

The derivation of the water vapour mole fraction $\mathrm{C_{H_2O_v}}$ from relative humidity, air temperature and air pressure from the low-cost thermohygrometer was also presented in Markwitz and Siebicke (2019) and is given in this section.

The water vapour mole fraction, $\mathrm{C_{H_2O_v}}$, was derived from the definition of the specific humidity, q, as the quantity of water vapour per quantity of moist air. The latter two quantities were expressed as the density of water vapour, $\rho_{\mathrm{H_2O_v}}$, and moist air,

ρ_m, respectively. The density of moist air is defined as the sum of the density of dry air, ρ_d, and the density of water vapour.

$$q = \frac{\rho_{H_2O_v}}{\rho_m} = \frac{\rho_{H_2O_v}}{\rho_d + \rho_{H_2O_v}} \tag{A4}$$

We then replaced the density of water vapour and the density of dry air in Eq. (A4) as per Eqs. (A5) and (A6), respectively,

$$\rho_{H_2O_v} = \frac{C_{H_2O_v} \cdot M_{H_2O_v}}{V_m} \tag{A5}$$

$$\rho_d = \frac{p - e_a}{R_d \cdot T} \tag{A6}$$

with the molar mass of water vapour, $\mathrm{M_{H_2O_v}}$ = 18.02 $\mathrm{g\,mol^{-1}}$, the molar volume of air

$$V_m = \frac{\Re \cdot T}{p} \,(\mathrm{m^3\,mol^{-1}}), \tag{A7}$$

the universal gas constant, $\Re$ = 8.314 $\mathrm{J\,mol^{-1}K^{-1}}$, and the specific gas constant of dry air, R_d = 287.058 $\mathrm{J\,kg^{-1}\,K^{-1}}$.

Solving Eq. (A4) for $\mathrm{C_{H_2O_v}}$ leads to the water vapour mole fraction

$$C_{H_2O_v} = \frac{q\,\Re\,(p - e_a)}{p\,M_{H_2O_v}\,R_d(1-q)}. \tag{A8}$$

The specific humidity in Eq. (A8) was calculated as a function of relative humidity, temperature and air pressure measurements from the thermohygrometer:

$$q = 0.622 \cdot \frac{e_a}{p} \tag{A9}$$

The actual vapour pressure, $\mathrm{e_a}$ (kPa), in Eq. (A9) was calculated from an approximation of the saturation vapour pressure, $\mathrm{e_*(T)}$ (Stull, 1989) and from relative humidity, RH,

$$e = \frac{RH \cdot e_*(T)}{100} \tag{A10}$$

$$e_*(T) = 0.6112 \exp\left(\frac{17.67T}{(T + 273.15) - 29.66}\right) \tag{A11}$$

A3 Canopy resistance

The Penman-Monteith equation for evapotranspiration of a canopy (Monteith, 1965) is

$$LE = \frac{s(R_N - G) + c_p\,D\,g_{ah}}{s + \gamma(1 + g_{ah}/g_c)} \tag{A12}$$

with the vapour pressure deficit, $\mathrm{D = e_*(T) - e_a}$ (hPa), the heat capacity at constant pressure, c_p = 1005 J $\mathrm{(kg\,K)^{-1}}$ and the psychrometer constant, $\gamma = (c_p\,P_A)/(L\,0.622)$.

The slope of the saturation vapour pressure curve, s, is

$$s = \frac{\varepsilon L q_{sat}}{R_v T} \tag{A13}$$

with $\varepsilon = 0.622$ and the specific humidity at saturation, $q_{sat} = \varepsilon e_*(T)/P_A)$ as a function of temperature.

Rearranging Eq. (A12) yields the canopy resistance, r_c ($\mathrm{s\,m^{-1}}$),

$$r_c = \frac{1}{g_c} = \frac{s/\gamma+1}{g_{ah}}\left[\frac{s/\gamma(R_N-G)}{(s/\gamma+1)LE}-1\right]+\frac{c_p D}{\gamma LE} \tag{A14}$$

The aerodynamic conductance for heat is

$$g_{ah} = \frac{1}{r_{ah}} = \frac{\kappa^2 u}{\left(\ln\left(\frac{z-d}{z_{0m}}\right)-\psi_m(\zeta)\right)\left(\ln\left(\frac{z-d}{z_{0h}}\right)-\psi_h(\zeta)\right)} \tag{A15}$$

with the von Karman constant, $\kappa = 0.4$, the horizontal wind velocity, u ($\mathrm{m\,s^{-1}}$), the measurement height, z (m), the displacement height, d (m), estimated as 70 % of the canopy height, the roughness length for momentum transport, $\mathrm{z_{0m}}$, estimated as 10 % of the canopy height and the roughness length for heat transport, $\mathrm{z_{0h}}$, estimated as 10 % of $\mathrm{z_{0m}}$. $\psi_\mathrm{m}(\zeta)$ is the universal function for momentum and $\psi_\mathrm{h}(\zeta)$ is the universal function for heat. $\psi_\mathrm{m}(\zeta)$ and $\psi_\mathrm{h}(\zeta)$ depend on atmospheric stability with the stability parameter $\zeta = (\mathrm{z}-\mathrm{d})/\mathrm{L}$, including the Monin-Obukhov length, L. ψ_m and ψ_h were calculated as

$$\psi_m(\zeta) = \begin{cases} 2\ln[(1+x)/2] + \ln[(1+x^2)/2] & \text{for } \zeta < 0 \\ -2\arctan(x) + \pi/2 & \\ & \\ -5\zeta & \text{for } \zeta \geq 0 \end{cases} \tag{A16}$$

$$\psi_h(\zeta) = \begin{cases} 2\ln[(1+x^2)/2] & \text{for } \zeta < 0 \\ -5\zeta & \text{for } \zeta \geq 0 \end{cases} \tag{A17}$$

with $\mathrm{x} = (1-16\zeta)^{1/4}$ (Bonan, 2016; Businger et al., 1971; Stull, 1989).

Appendix B: Tables

Table A1. Temporal extent of the EC measurement campaigns.

Site	Campaign period
Dornburg MC	16 June to 14 July 2016
Donburg AF	14 July to 12 August 2016
Reiffenhausen AF	12 August to 14 September 2016
Wendhausen	03 May to 02 June 2017
Forst	08 June to 08 July 2017
Mariensee	21 July to 19 September 2017

Table A2. Site specific soil characteristics, with the soil texture being representative for the top soil column of 0.3 m. The bulk density is representative for the top soil column of 0.05 m. Data provided by Göbel et al. (2018) and Marcus Schmidt (pers. comm., Georg August University of Goettingen, Buesgen Institute, Soil Science of Tropical and Subtropical Ecosystems).

Site	Clay content (%)	Sand content (%)	Bulk density ($kg\,m^{-3}$)
Dornburg AF	20.5	3.75	1.22
Dornburg MC	38	10.75	1.19
Forst AF	7	60.75	1.3
Forst MC	9.5	66.75	1.28
Mariensee AF	11.75	48	–
Mariensee MC	31.67	54.33	1.28
Reiffenhausen AF	23.75	31.5	1.28
Reiffenhausen MC	22.75	49.75	1.28
Wendhausen AF	35	18.25	1.085
Wendhausen MC	44.5	27	0.89

Appendix B: Figures

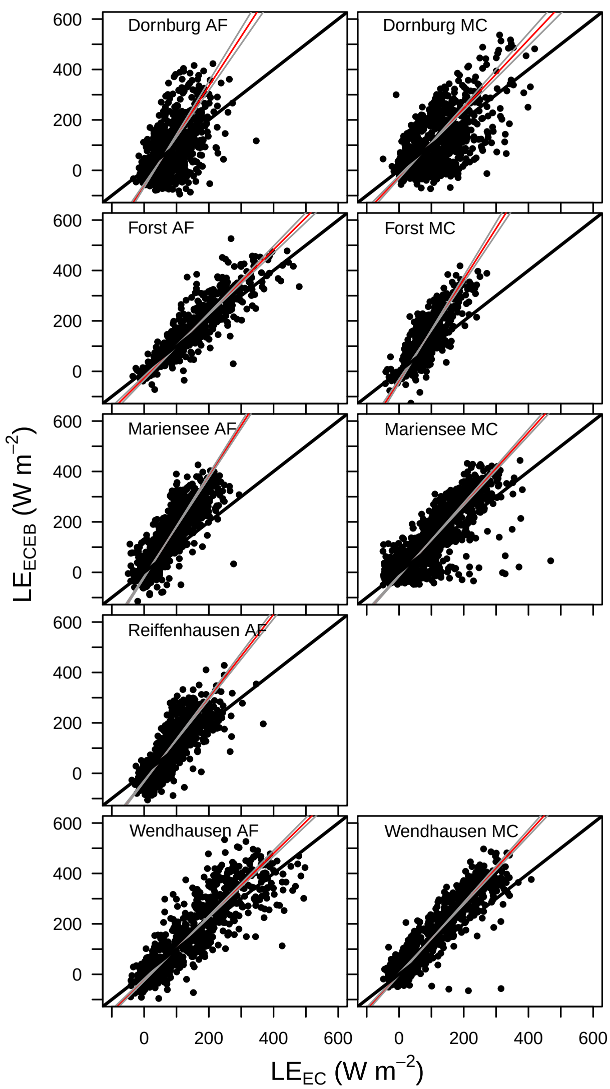

Figure A1. Scatter plot of LE_{ECEB} versus LE_{EC} for all sites. The red line denotes the best fit line with grey lines the ±2.5 % confidence interval lines and the solid black lines corresponds to the 1:1 line. Data from Reiffenhausen MC are missing due to the unavailability of a campaign.

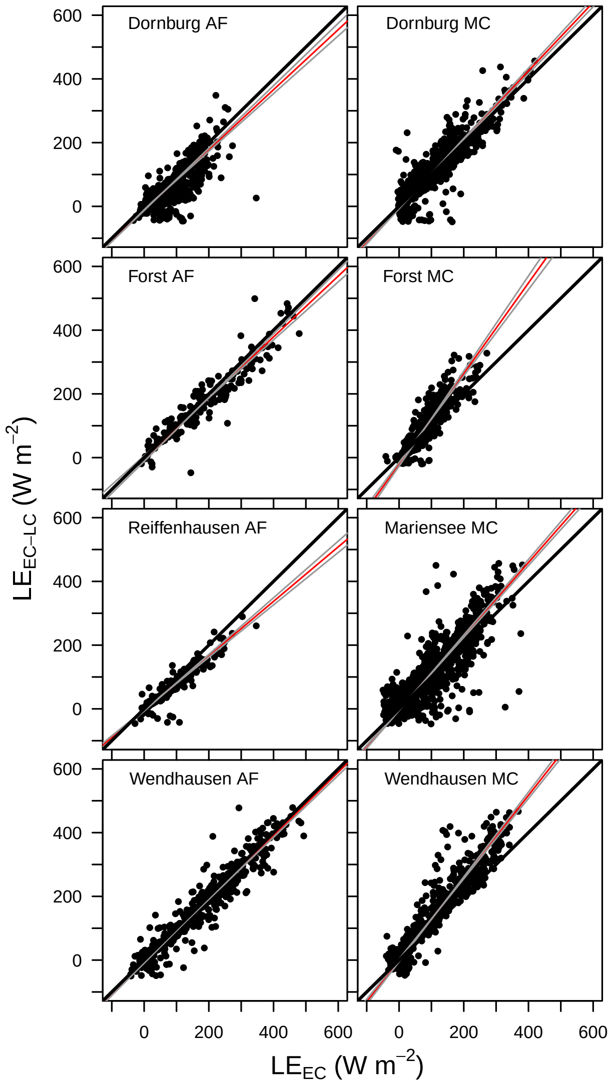

Figure A2. Scatter plot of $\mathrm{LE_{EC-LC}}$ versus $\mathrm{LE_{EC}}$ for all sites. The red line denotes the best fit line with grey lines the ± 2.5 % confidence interval lines and the solid black lines corresponds to the 1:1 line. Data from Reiffenhausen MC are missing due to the unavailability of a campaign and $\mathrm{LE_{EC-LC}}$ from Mariensee AF is missing due to sensor malfunctions.

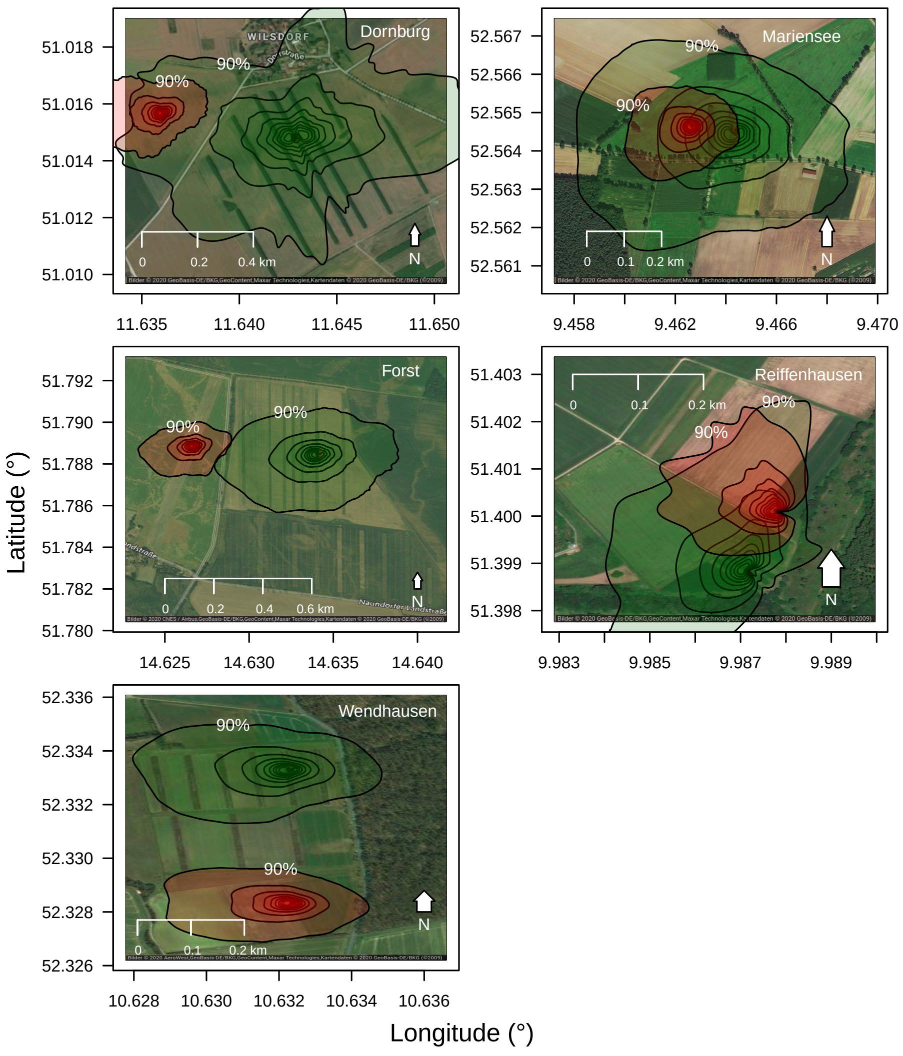

Figure A3. Flux footprint climatology for all sites and all available data during the years 2016 and 2017. Green shaded footprints correspond to the agroforestry system and red shaded footprints correspond to the monoculture system. For the analysis only daytime data were used ($R_G > 20$ $\mathrm{Wm}{-2}$). Aerial photographs originate from Google maps/ Google earth ©Google 2020.

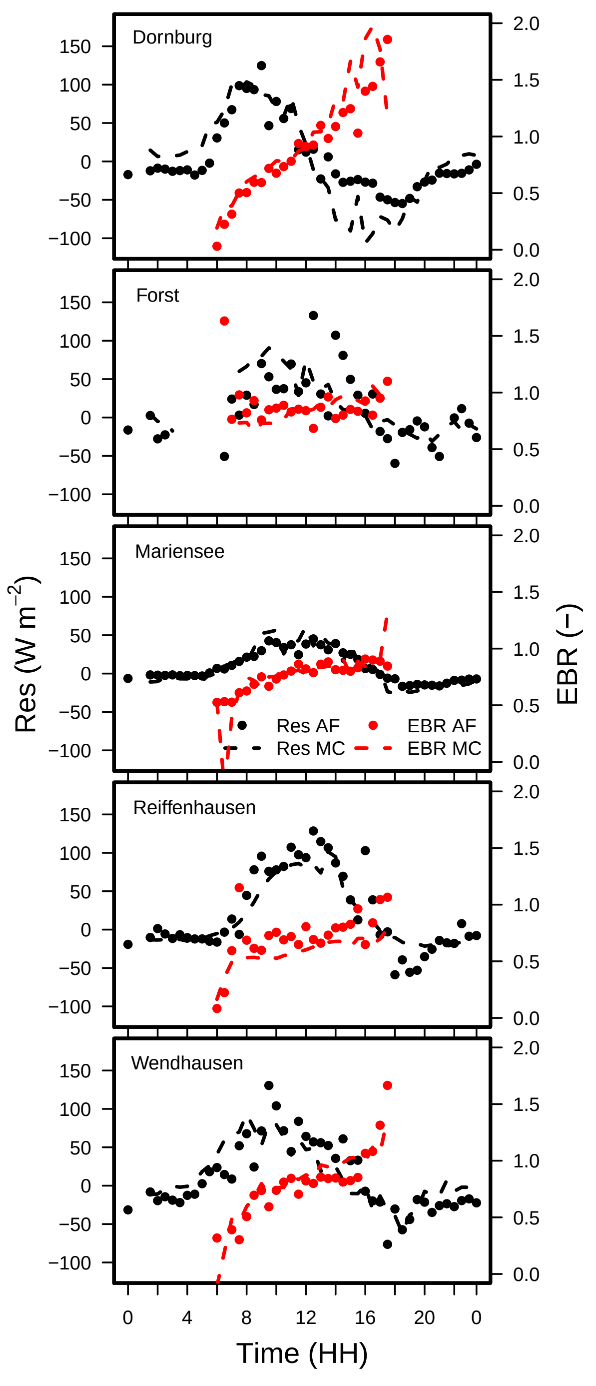

Figure A4. Median diel cycle of the energy balance ratio (EBR) and diurnal cycle of the residual energy for the AF and the MC systems at all sites. LE was obtained by EC-LC. Data from Mariensee AF are from 23 March 2016 to 20 November 2016 and at Reiffenhausen MC the analyses are based on data collected from 07 April 2016 to 31 December 2016, because no data were available during the campaigns.

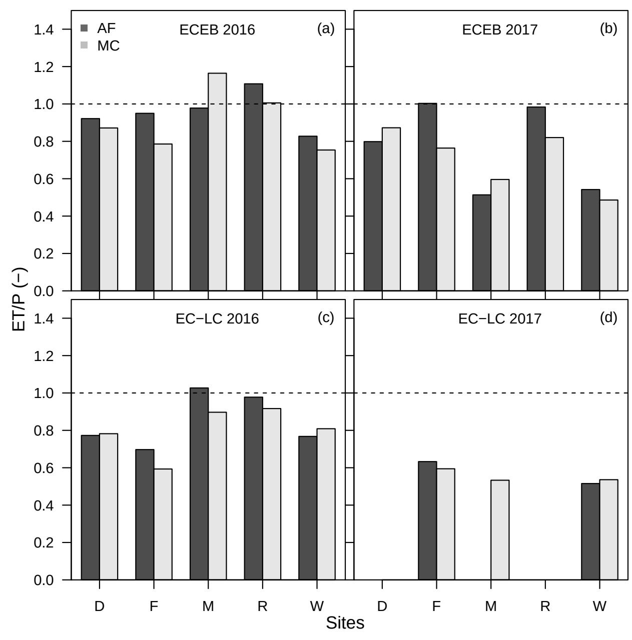

Figure A5. Bar plot of the evapotranspiration index for the ECEB method for the years 2016, a, and 2017, b, and for the EC-LC method for 2016, c, and 2017, d, for sites, e.g., Dornburg, "D", Forst, "F", Mariensee, "M", Reiffenhausen, "R", and Wendhausen, "W". The dashed line indicates a evapotranspiration index of one. Evapotranspiration indices for Dornburg AF and MC, Mariensee AF, Reiffenhausen AF and MC in 2017 are missing due to instrument malfunctions.

References

Amiro, B.: Measuring boreal forest evapotranspiration using the energy balance residual, J. Hydrol., 366, 112–118, https://doi.org/10.1016/j.jhydrol.2008.12.021, 2009.

Aubinet, M., Feigenwinter, C., Heinesch, B., Bernhofer, C., Canepa, E., Lindroth, A., Montagnani, L., Rebmann, C., Sedlak, P., and Van Gorsel, E.: Direct advection measurements do not help to solve the night-time CO2 closure problem: Evidence from three different forests, Agric. For. Meteorol., 150, 655–664, https://doi.org/10.1016/j.agrformet.2010.01.016, 2010.

Aylott, M. J., Casella, E., Tubby, I., Street, N. R., Smith, P., and Taylor, G.: Yield and spatial supply of bioenergy poplar and willow short-rotation coppice in the UK, New Phytol., 178, 358–370, https://doi.org/10.1111/j.1469-8137.2008.02396.x, 2008.

Baldocchi, D.: Measuring fluxes of trace gases and energy between ecosystems and the atmosphere - the state and future of the eddy covariance method, Glob. Chang. Biol., 20, 3600–3609, https://doi.org/10.1111/gcb.12649, 2014.

Baldocchi, D. D.: Assessing the eddy covariance technique for evaluating carbon dioxide exchange rates of ecosystems: past, present and future, Glob. Chang. Biol., 9, 479–492, https://doi.org/10.1046/j.1365-2486.2003.00629.x, 2003.

Beuschel, R., Piepho, H.-P., Joergensen, R. G., and Wachendorf, C.: Similar spatial patterns of soil quality indicators in three poplar-based silvo-arable alley cropping systems in Germany, Biol. Fertil. Soils, https://doi.org/10.1007/s00374-018-1324-3, 2018.

Bloemen, J., Fichot, R., Horemans, J. A., Broeckx, L. S., Verlinden, M. S., Zenone, T., and Ceulemans, R.: Water use of a multigenotype poplar short-rotation coppice from tree to stand scale, GCB Bioenergy, https://doi.org/10.1111/gcbb.12345, 2016.

Boessenkool, B.: Package ‘ rdwd ’: Select and Download Climate Data from ’DWD’ (German Weather Service), Tech. rep., Potsdam University, Department of geoecology, https://cran.r-project.org/web/packages/rdwd/vignettes/rdwd.html, 2019.

Böhm, C., Kanzler, M., and Freese, D.: Wind speed reductions as influenced by woody hedgerows grown for biomass in short rotation alley cropping systems in Germany, Agrofor. Syst., 88, 579–591, https://doi.org/10.1007/s10457-014-9700-y, 2014.

Bonan, G.: Ecological Climatology - Concepts and applications, Cambridge University Press, 3 edn., 2016.

Budyko, M. I.: Climate and life, Acadamic Press, New York, 1974.

Businger, J. a., Wyngaard, J. C., Izumi, Y., and Bradley, E. F.: Flux-Profile Relationships in the Atmospheric Surface Layer, https://doi.org/10.1175/1520-0469(1971)028<0181:FPRITA>2.0.CO;2, 1971.

Chen, T. and Guestrin, C.: XGBoost: A Scalable Tree Boosting System, J. Assoc. Physicians India, pp. 1–10, https://doi.org/10.1145/2939672.2939785, 2016.

Chen, T., He, T., Benesty, M., Khotilovich, V., Tang, Y., Cho, H., Chen, K., Rory Mitchell, Cano, I., Zhou, T., Li, M., Xie, J., Lin, M., Geng, Y., and Li, Y.: Package ’xgboost’ - Extreme Gradient Boosting, https://xgboost.readthedocs.io/en/latest/, 2019.

Cleugh, H. A.: Effects of windbreaks on airflow, microclimates and crop yields, Agrofor. Syst., 41, 55–84, https://doi.org/10.1023/A:1006019805109, 1998.

Dake, J. M. K.: Evaporative cooling of a body of water, Water Resour. Res., 8, 1087–1091, https://doi.org/doi:10.1029/WR008i004p01087, 1972.

Davis, J. E. and Norman, J. M.: 22. Effects of shelter on plant water use, Agric. Ecosyst. Environ., 22-23, 393–402, https://doi.org/10.1016/0167-8809(88)90034-5, 1988.

De Stefano, A. and Jacobson, M. G.: Soil carbon sequestration in agroforestry systems: a meta-analysis, Agrofor. Syst., 92, 285–299, https://doi.org/10.1007/s10457-017-0147-9, 2018.

Falge, E., Baldocchi, D., Olson, R., Anthoni, P., Aubinet, M., Bernhofer, C., Burba, G., Ceulemans, R., Clement, R., Dolman, H., Granier, A., Gross, P., Grünwald, T., Hollinger, D., Jensen, N. O., Katul, G., Keronen, P., Kowalski, A., Lai, C. T., Law, B. E., Meyers, T., Moncrieff, J., Moors, E., Munger, J. W., Pilegaard, K., Rannik, Ü., Rebmann, C., Suyker, A., Tenhunen, J., Tu, K., Verma, S., Vesala, T., Wilson, K., and Wofsy, S.: Gap filling strategies for defensible annual sums of net ecosystem exchange, Agric. For. Meteorol., 107, 43–69, https://doi.org/10.1016/S0168-1923(00)00225-2, 2001.

Fischer, M., Trnka, M., Kučera, J., Deckmyn, G., Orság, M., Sedlák, P., Žalud, Z., and Ceulemans, R.: Evapotranspiration of a high-density poplar stand in comparison with a reference grass cover in the Czech-Moravian Highlands, Agric. For. Meteorol., 181, 43–60, https://doi.org/10.1016/j.agrformet.2013.07.004, 2013.

Fischer, M., Zenone, T., Trnka, M., Orság, M., Montagnani, L., Ward, E. J., Tripathi, A. M., Hlavinka, P., Seufert, G., Žalud, Z., King, J. S., and Ceulemans, R.: Water requirements of short rotation poplar coppice: Experimental and modelling analyses across Europe, Agric. For. Meteorol., 250-251, 343–360, https://doi.org/10.1016/j.agrformet.2017.12.079, 2018.

Foken, T.: The Energy Balance Closure Problem: an Overview, Ecol. Appl., 18, 1351–1367, https://doi.org/10.1890/06-0922.1, 2008a.

Foken, T.: Micrometorology, vol. 1, Springer-Verlag Berlin Heidelberg, Bayreuth, 2008b.

Foken, T., Wimmer, F., Mauder, M., Thomas, C., and Liebethal, C.: Some aspects of the energy balance closure problem, Atmos. Chem. Phys. Discuss., 6, 3381–3402, https://doi.org/10.5194/acpd-6-3381-2006, 2006.

Göbel, L., Corre, M. D., Veldkamp, E., and Schmidt, M.: BonaRes SIGNAL, Site: Mariensee and Reiffenhausen, soil characteristics, https://doi.org/10.20387/BonaRes-FQ8B-031J, 2018.

Hill, T., Chocholek, M., and Clement, R.: The case for increasing the statistical power of eddy covariance ecosystem studies: why, where and how?, Glob. Chang. Biol., 23, 2154–2165, https://doi.org/10.1111/gcb.13547, 2017.

Hollinger, D. Y. and Richardson, A. D.: Uncertainty in eddy covariance measurements and its application to physiological models, Tree Physiol., 25, 873–885, https://doi.org/10.1093/treephys/25.7.873, 2005.

Imukova, K., Ingwersen, J., Hevart, M., and Streck, T.: Energy balance closure on a winter wheat stand: Comparing the eddy covariance technique with the soil water balance method, Biogeosciences, 13, 63–75, https://doi.org/10.5194/bg-13-63-2016, 2016.

Jacobs, A. F. G., Heusinkveld, B. G., and Holtslag, A. A. M.: Towards closing the surface energy budget of a mid-latitude grassland, Boundary-Layer Meteorol., 126, 125–136, https://doi.org/10.1007/s10546-007-9209-2, 2008.

Kanzler, M., Böhm, C., Mirck, J., Schmitt, D., and Veste, M.: Microclimate effects on evaporation and winter wheat (Triticum aestivum L.) yield within a temperate agroforestry system, Agrofor. Syst., 4, https://doi.org/10.1007/s10457-018-0289-4, 2018.

Katul, G. G., Oren, R., Manzoni, S., Higgins, C., and Parlange, M. B.: Evapotranspiration: a process driving mass transport and energy exchnge in the soil-plant-atmosphere-climate system, Rev. Geophys., 50, RG000 366: 1—-25, https://doi.org/10.1029/2011RG000366.1.INTRODUCTION, 2012.

Kljun, N., Calanca, P., Rotach, M. W., and Schmid, H. P.: A simple two-dimensional parameterisation for Flux Footprint Prediction (FFP), Geosci. Model Dev., 8, 3695–3713, https://doi.org/10.5194/gmd-8-3695-2015, 2015.

Liebethal, C. and Foken, T.: Evaluation of six parameterization approaches for the ground heat flux, Theor. Appl. Climatol., 88, 43–56, https://doi.org/10.1007/s00704-005-0234-0, 2007.

Lindroth, A.: Aerodynamic and canopy resistance of short-rotation forest in relation to leaf area index and climate, Boundary-Layer Meteorol., 66, 265–279, https://doi.org/10.1007/BF00705478, 1993.

Malec, S.: University of Kassel, Grassland Science and Renewable Plant Resources. Unpublished data., 2017.

Markwitz, C. and Siebicke, L.: Low-cost eddy covariance: a case study of evapotranspiration over agroforestry in Germany, Atmos. Meas. Tech., 12, 4677–4696, https://doi.org/10.5194/amt-12-4677-2019, 2019.

McNaughton, K. G.: 1. Effects of windbreaks on turbulent transport and microclimate, Agric. Ecosyst. Environ., 22-23, 17–39, https://doi.org/10.1016/0167-8809(88)90006-0, 1988.

Moncrieff, J., Massheder, J., de Bruin, H., Elbers, J., Friborg, T., Heusinkveld, B., Kabat, P., Scott, S., Soegaard, H., and Verhoef, A.: A system to measure surface fluxes of momentum, sensible heat, water vapour and carbon dioxide, J. Hydrol., 188-189, 589–611, https://doi.org/10.1016/S0022-1694(96)03194-0, 1997.

Monteith, J. L.: Evaporation and environment, Symp. Soc. Exp. Biol., 19, 205–234, 1965.

Morhart, C. D., Douglas, G. C., Dupraz, C., Graves, A. R., Nahm, M., Paris, P., Sauter, U. H., Sheppard, J., and Spiecker, H.: Alley coppice-a new system with ancient roots, Ann. For. Sci., 71, 527–542, https://doi.org/10.1007/s13595-014-0373-5, 2014.

Nuberg, I. K.: Effect of shelter on temperate crops: A review to define research for Australian conditions, Agrofor. Syst., 41, 3–34, https://doi.org/10.1023/A:1006071821948, 1998.

Oncley, S. P., Foken, T., Vogt, R., Kohsiek, W., DeBruin, H. A., Bernhofer, C., Christen, A., van Gorsel, E., Grantz, D., Feigenwinter, C., Lehner, I., Liebethal, C., Liu, H., Mauder, M., Pitacco, A., Ribeiro, L., and Weidinger, T.: The energy balance experiment EBEX-2000. Part I: Overview and energy balance, Boundary-Layer Meteorol., 123, 1–28, https://doi.org/10.1007/s10546-007-9161-1, 2007.

Quinkenstein, A., Wöllecke, J., Böhm, C., Grünewald, H., Freese, D., Schneider, B. U., and Hüttl, R. F.: Ecological benefits of the alley cropping agroforestry system in sensitive regions of Europe, Environ. Sci. Policy, 12, 1112–1121, https://doi.org/10.1016/j.envsci.2009.08.008, 2009.

Reichstein, M., Falge, E., Baldocchi, D., Papale, D., Aubinet, M., Berbigier, P., Bernhofer, C., Buchmann, N., Gilmanov, T., Granier, A., Grünwald, T., Havránková, K., Ilvesniemi, H., Janous, D., Knohl, A., Laurila, T., Lohila, A., Loustau, D., Matteucci, G., Meyers, T., Miglietta, F., Ourcival, J. M., Pumpanen, J., Rambal, S., Rotenberg, E., Sanz, M., Tenhunen, J., Seufert, G., Vaccari, F., Vesala, T., Yakir, D., and Valentini, R.: On the separation of net ecosystem exchange into assimilation and ecosystem respiration: Review and improved algorithm, Glob. Chang. Biol., 11, 1424–1439, https://doi.org/10.1111/j.1365-2486.2005.001002.x, 2005.

Rudolf, C.: Thurengian state office of agriculture and rural areas. Unpublished data., 2017.

Schmid, H. P.: Footprint modeling for vegetation atmosphere exchange studies: A review and perspective, Agric. For. Meteorol., 113, 159–183, https://doi.org/10.1016/S0168-1923(02)00107-7, 2002.

Schmidt-Walter, P., Richter, F., Herbst, M., Schuldt, B., and Lamersdorf, N. P.: Transpiration and water use strategies of a young and a full-grown short rotation coppice differing in canopy cover and leaf area, Agric. For. Meteorol., 195-196, 165–178, https://doi.org/10.1016/j.agrformet.2014.05.006, 2014.

Seserman, D.-M.: Brandenburg University of Technology, Cottbus-Senftenberg, Soil protection and recultivation. Unpublished data., 2017.

Smith, J., Pearce, B. D., and Wolfe, M. S.: Reconciling productivity with protection of the environment: Is temperate agroforestry the answer?, Renew. Agric. Food Syst., 28, 80–92, https://doi.org/10.1017/S1742170511000585, 2013.

Stoy, P. C., Mauder, M., Foken, T., Marcolla, B., Boegh, E., Ibrom, A., Arain, M. A., Arneth, A., Aurela, M., Bernhofer, C., Cescatti, A., Dellwik, E., Duce, P., Gianelle, D., van Gorsel, E., Kiely, G., Knohl, A., Margolis, H., Mccaughey, H., Merbold, L., Montagnani, L., Papale, D., Reichstein, M., Saunders, M., Serrano-Ortiz, P., Sottocornola, M., Spano, D., Vaccari, F., and Varlagin, A.: A data-driven analysis of energy balance closure across FLUXNET research sites: The role of landscape scale heterogeneity, Agric. For. Meteorol., 171-172, 137–152, https://doi.org/10.1016/j.agrformet.2012.11.004, 2013.

Stull, R. B.: An introduction to boundary layer meteorology, Kluwer Academic Publishers, https://doi.org/10.1007/978-94-009-3027-8, 1989.

Swieter, A. and Langhof, M.: Julius Kühn-Institut, Institute for crop and soil science. Unpublished data, 2017.

Swieter, A., Langhof, M., Lamerre, J., and Greef, J. M.: Long-term yields of oilseed rape and winter wheat in a short rotation alley cropping agroforestry system, Agrofor. Syst., 93, 1853–1864, https://doi.org/10.1007/s10457-018-0288-5, 2019.

Tsonkova, P., Böhm, C., Quinkenstein, A., and Freese, D.: Ecological benefits provided by alley cropping systems for production of woody biomass in the temperate region: a review, Agrofor. Syst., 85, 133–152, https://doi.org/10.1007/s10457-012-9494-8, 2012.

Twine, T. E., Kustas, W. P., Norman, J. M., Cook, D. R., Houser, P. R., Meyers, T. P., Prueger, J. H., Starks, P. J., and Wesely, M. L.: Correcting eddy-covariance flux underestimates over a grassland, Agric. For. Meteorol., 103, 279–300, https://doi.org/10.1016/S0168-1923(00)00123-4, 2000.

Ward, P. R., Micin, S. F., and Fillery, I. R. P.: Application of eddy covariance to determine ecosystem-scale carbon balance and evapotranspiration in an agroforestry system, Agric. For. Meteorol., 152, 178–188, https://doi.org/10.1016/j.agrformet.2011.09.016, 2012.

Webster, R.: Regression and functional relations, Eur. J. Soil Sci., 48, 557–566, https://doi.org/10.1111/j.1365-2389.1997.tb00222.x, 1997.

Williams, C. A., Reichstein, M., Buchmann, N., Baldocchi, D., Beer, C., Schwalm, C., Wohlfahrt, G., Hasler, N., Bernhofer, C., Foken, T., Papale, D., Schymanski, S., and Schaefer, K.: Climate and vegetation controls on the surface water balance: Synthesis of evapotranspiration measured across a global network of flux towers, Water Resour. Res., 48, 1–13, https://doi.org/10.1029/2011WR011586, 2012.

Zenone, T., Fischer, M., Arriga, N., Broeckx, L. S., Verlinden, M. S., Vanbeveren, S., Zona, D., and Ceulemans, R.: Biophysical drivers of the carbon dioxide, water vapor, and energy exchanges of a short-rotation poplar coppice, Agric. For. Meteorol., 209-210, 22–35, https://doi.org/10.1016/j.agrformet.2015.04.009, 2015.